Universiteit
Leiden
The Netherlands

Chemical genetic approaches for target validation

Wel, T. van der

Citation
Wel, T. van der. (2020, January 22). *Chemical genetic approaches for target validation*. Retrieved from https://hdl.handle.net/1887/83257

Version:	Publisher's Version
License:	Licence agreement concerning inclusion of doctoral thesis in the Institutional Repository of the University of Leiden
Downloaded from:	https://hdl.handle.net/1887/83257

Note: To cite this publication please use the final published version (if applicable).

Cover Page

Universiteit Leiden

The handle http://hdl.handle.net/1887/83257 holds various files of this Leiden University dissertation.

Author: Wel, T. van der
Title: Chemical genetic approaches for target validation
Issue Date: 2020-01-22

2

A chemical genetic strategy for visualization of engineered kinases and their target engagement by covalent complementary probes

Introduction

Protein kinases comprise a 518-membered family of enzymes that play an essential role in intracellular signaling processes. They transfer a phosphate group from ATP to specific amino acid residues in proteins, thereby modulating protein activity, localization and protein-protein interactions.[1,2] Protein kinases are involved in many cellular functions, including proliferation, differentiation, migration and host-pathogen interactions. Kinases are also an important class of drug targets for the treatment of cancer.[3] However, current FDA-approved kinase inhibitors intend to target only <5% of the entire kinome[4] and therapeutic indications outside oncology are vastly underrepresented.[5,6] These so-far untargeted kinases thus offer great opportunities for the development of novel molecular therapies for various diseases. The non-receptor tyrosine kinase feline sarcoma oncogene (FES), subject of this study, is a potential therapeutic target for cancer and immune disorders.[7–9]

FES has a restricted expression pattern and is primarily found in hematopoietic, neuronal, endothelial and epithelial cells.[10] FES, together with FES-related kinase (FER), constitutes a distinct subgroup within the family of tyrosine kinases, defined by their unique structural organization (Figure 2.1A). FES is able to interact via its F-Bin-Amphiphysin-Rvs (F-BAR) domain, either with itself or other F-BAR-containing proteins.[11] These interactions are proposed to maintain an inactive conformation in absence of activating stimuli.[12] The FES F-BAR domain binds to phosphoinositide-containing lipids, such as phosphatidylinositol 4,5-bisphosphate (PIP_2). In addition, phosphatidic acid binding via the F-BAR extension (FX) domain can increase kinase activity, although the exact mechanism remains poorly understood.[13] FES also possesses a Src Homology 2 (SH2) domain that binds phosphorylated tyrosine residues and thereby functions as protein interaction domain. Moreover, electrostatic interactions between the SH2 domain and adjacent kinase domain of FES are essential to adopt an active conformation required for catalysis and disruption of this SH2-kinase domain interface severely impairs kinase activity.[14] The kinase domain that performs the transfer of phosphate groups from ATP to protein substrates is located on the C-terminal end of FES. Phosphorylation of Y713 in the activation loop of FES is a prerequisite for its kinase activity[15] and can occur either via autophosphorylation[16] or phosphorylation by Src family kinases.[17] Upon activating stimuli, FES translocates to the membrane to form oligomers, followed by autophosphorylation at Y713, after which FES adopts an active conformation suitable for catalysis (Figure 2.1B).[18]

The successful development of new drugs targeting kinases strongly depends on the understanding of their underlying molecular and cellular mechanism of action, *i.e.* the preclinical target validation.[19] The physiological function of many kinases remains, however, poorly characterized and their direct protein substrates are often unknown.

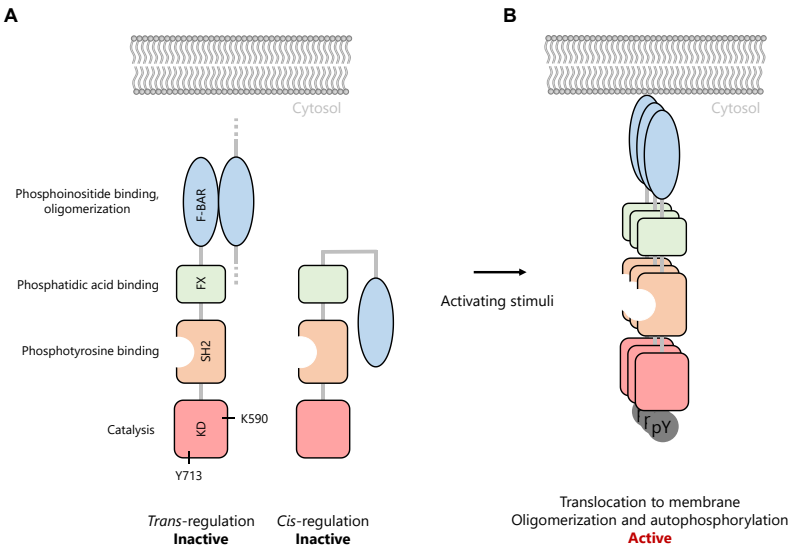

Figure 2.1 – Structural domains of FES and regulation of FES activity. (A) FES has a unique structural organization consisting of an F-Bin-Amphiphysin-Rvs (F-BAR), F-BAR extension (FX), Src Homology 2 (SH2) and kinase domain (KD). FES is present in an inactive conformation in absence of activation stimuli. K590 is the catalytic lysine residue that forms a salt bridge with E607 to adopt an active conformation. Y713 in the activation loop of FES is an autophosphorylation site that increases kinase activity. **(B)** Upon activation stimuli, FES translocates to the membrane, resulting in oligomerization via its F-BAR domain. FES is then activated by autophosphorylation of its Y713 residue.

Genetic models (congenital deletion or expression of kinase-dead variants) may be used to study these questions (Figure 2.2A). However, the interpretation of results from long-term, constitutive genetic disruption may sometimes be hampered by potential compensatory mechanisms. In addition, these models are poorly suited to dissect rapid and dynamic catalytic processes from the scaffolding function of kinases.[20,21] A complementary approach is the use of small molecule inhibitors to modulate kinase activity in an acute and temporal fashion. This approach more closely resembles therapeutic intervention, but the available pharmacological tools, especially for non-validated kinases, often suffer from a lack of selectivity.[20,22] Currently, there are no suitable FES inhibitors available for target validation studies, because they either lack potency or selectivity and all cross-react with FER.[7,23]

Another important aspect of drug discovery is to obtain proof of target engagement, which correlates the exposure at the site of action to a pharmacological or phenotypic readout.[24] Information about kinase engagement is essential for determining the dose required for full target occupancy without inducing undesired off-target activity.[25] Activity- and affinity-based protein profiling is a chemical biology technique that is ideally suited to study target engagement.[24] Chemical probes make use of a covalent, irreversible mode of action, combined with reporter tags such as fluorophores to enable target visualization or biotin to enable target enrichment and identification. In the field of kinases,

reported chemical probes either target a conserved active site lysine residue in a non-selective fashion[26] or non-catalytic cysteine residues in the ATP binding pocket.[27,28] The first class of kinase ABPs lacks the selectivity required for cellular target engagement studies. On the other hand, the majority of kinases, including FES, do not possess targetable cysteine residues in the catalytic pocket[29]. Garske *et al.* previously introduced the elegant concept of covalent complementarity: the use of an engineered kinase in which the gatekeeper amino acid residue is mutated into a cysteine, combined with electrophilic ATP analogs to study target engagement.[30] Other positions in the kinase active site have also been investigated[31,32], but secondary mutations were required to improve cysteine reactivity or compound selectivity and potency.

Inspired by these established and emerging concepts, in this study, a chemical genetic strategy was developed to visualize target engagement of kinases and aid in their validation as potential therapeutic targets.

Results

General strategy: an engineered kinase in combination with complementary probes

The key feature of the strategy is the combination of an engineered, mutant kinase with the design and application of complementary, covalent inhibitors (Figure 2.2B). The ATP-binding pocket of the kinase of interest is sensitized towards pharmacological inactivation using complementary probes by replacing an amino acid for a cysteine residue. Candidate mutants are rationally designed *in silico* using existing structural data, taking into account residue accessibility and avoiding mutagenesis of residues essential for catalysis (Figure 2.2C, step 1). The mutant is biochemically characterized to verify that the cysteine point mutation minimally affects kinase function (Figure 2.2C, step 2). Subsequently, complementary electrophilic inhibitors are designed to covalently react with this cysteine (Figure 2.2C, step 3). Covalent, irreversible inhibitors can have several advantages over reversible compounds, such as sustained target occupancy, lower susceptibility to competition by high intracellular ATP concentrations and a pharmacodynamic profile that is dependent on the target's *de novo* protein synthesis rate[33,34]. The inhibitor will have far lower potency on the wild-type kinase, which does not possess a nucleophilic residue in its active site, thereby making the inhibitor mutant-specific. Transient overexpression of the mutant kinase allows *in situ* target engagement profiling in live cells, while the wild-type kinase serves as a negative control (Figure 2.2C, step 4). Importantly, the covalent binding mode of the inhibitor enables target engagement profiling by acting as a chemical probe and its ligation handle can be further functionalized with reporter tags for visualization by SDS-PAGE (fluorophore) or identification of the bound targets by mass spectrometry (biotin) (Figure 2.2C, step 5).

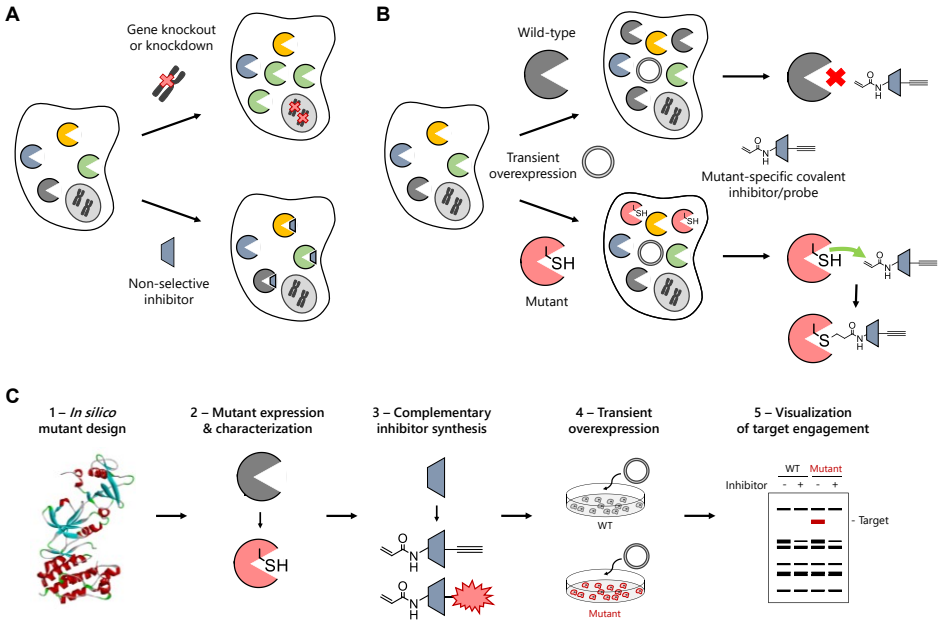

Figure 2.2 – Chemical genetic strategy for visualization of kinase target engagement. (A) Gene knockout or knockdown approaches suffer from a lack of temporal control, possibly inducing compensatory mechanisms such as upregulation of other kinases. On the other hand, many kinase inhibitors suffer from selectivity issues, leading to inactivation of multiple kinases and thereby resulting in a complex phenotype. **(B)** Chemical genetic strategy involving mutagenesis of a kinase active site residue into a nucleophilic cysteine accompanied by mutant-specific covalent inhibitor design. A non-selective, reversible inhibitor is modified with an acrylamide electrophile to covalently react with the introduced cysteine, along with an alkyne ligation handle for conjugation to reporter tags using click chemistry. **(C)** Schematic workflow encompassing mutant design, expression and characterization, the design and synthesis of complementary inhibitors, transient expression of the wild-type or mutant kinase and visualization of target engagement by inhibitors using fluorescent probes.

Biochemical characterization of engineered FES kinases

To introduce a cysteine residue at an appropriate position in the ATP-binding pocket of FES, a previously reported crystal structure of FES with reversible inhibitor TAE684 (compound **1**) (PDB: 4e93) was inspected.[23] Nine active site residues situated in proximity of the bound ligand were selected (Figure 2.3A) and the respective cysteine point mutants were generated by site-directed mutagenesis on truncated human *FES* fused to an N-terminal His-tag. The wild-type protein and the mutants were recombinantly expressed in *Escherichia coli* (*E. coli*), purified using Ni^{2+}-affinity chromatography and tested for catalytic activity using a time-resolved fluorescence resonance energy transfer (TR-FRET) assay (Figure 2.3B).[35,36] Four of the nine tested mutants did not display any catalytic activity, including G570C (located on P-loop) and G642C (hinge region). Three mutants near the kinase hydrophobic backpocket (I567C, V575C and L638C) retained partial activity, whereas only two mutants (T646C and S700C) displayed catalytic activity similar to wild-type FES.

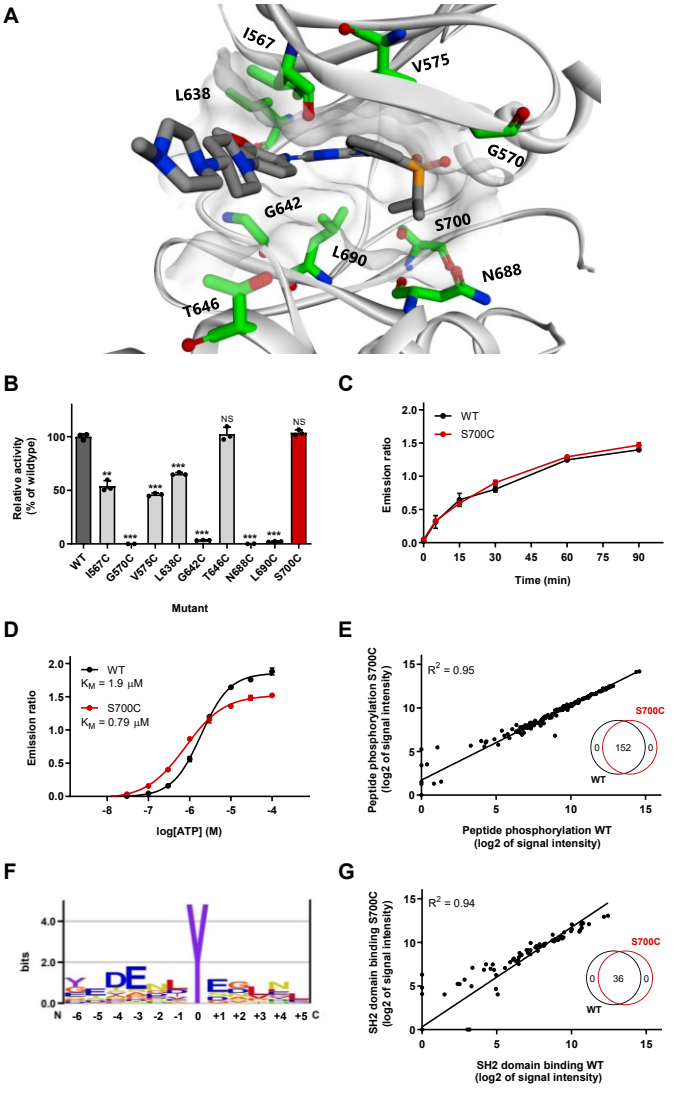

Figure 2.3 - Design and characterization of FES cysteine point mutants. (A) Location of mutated active site residues in FES crystal structure with bound reversible inhibitor TAE684 (PDB code: 4e93). **(B)** Activity of recombinantly expressed FES mutants compared to wild-type, determined as relative amount of phosphorylated peptide substrate after 60 min incubation using TR-FRET assay. **(C)** Reaction progress curve for FES^{WT} and FES^{S700C}. **(D)** Determination of ATP K_M for FES^{WT} and FES^{S700C}. Enzyme reactions in TR-FRET assays were performed with U*Light*-TK peptide (50 nM) and ATP (B, C: 100 µM, D: variable) and quenched (B, D: after 60 min, C: variable). **(E)** Peptide substrate profile for FES^{WT} and FES^{S700C} as determined in PamChip® microarray. Peptides were filtered for those with ATP-dependent signal and log2 of signal intensity >3. The peptide substrates were identical for FES^{WT} and FES^{S700C} (Venn diagram, inset). **(F)** Preferred substrate consensus sequence based on FES^{WT} substrate profile. Illustration was rendered using Enologos (http://www.benoslab.pitt.edu). **(G)** SH2 domain binding profile for FES^{WT} and FES^{S700C} as determined in PamChip® microarray. Samples with non-specific antibody binding were excluded. The peptide SH2 binding partners were identical for FES^{WT} and FES^{S700C} (Venn diagram, inset). Data represent means ± SEM (N = 3). Statistical analysis was performed using ANOVA with Holm-Sidak's multiple comparisons correction: *** P <0.001; NS if P >0.05.

The attention was particularly drawn to the S700C mutant, which involves the residue adjacent to the highly conserved DFG motif (DFG-1). Since several other kinases (*e.g.* MAPK1/3[37], RSK1-4[38] and TAK1[39]) express an endogenous cysteine at DFG-1 that can be targeted by electrophilic traps, FES^{S700C} was selected for more detailed biochemical profiling. The engineered kinase displayed identical reaction progress kinetics (Figure 2.3C) and similar affinity for ATP (K_M = 1.9 µM for FES^{WT} and K_M = 0.79 µM for FES^{S700C}; Figure 2.3D and Supplementary Figure 2.1A).

To assess whether the introduced mutation affected substrate recognition, a comparative substrate profiling assay was performed using the PamChip® microarray technology. This assay is based on the phosphorylation of immobilized peptides by purified FES and detection using a fluorescent phosphotyrosine antibody. Strikingly, the substrate profiles of FES^{WT} and FES^{S700C} were completely identical (Figure 2.3E, inset; Supplementary Table 2.1), indicating that the S700C mutation did not affect substrate recognition. Moreover, the absolute peptide phosphorylation levels showed a strong correlation (R^2 = 0.95). Sequence analysis of the top 30 of highest signal peptides revealed that FES prefers negatively charged substrates with hydrophobic residues at positions -1 and +3 and acidic residues at position -4, -3 and +1 relative to the tyrosine phosphorylation site (Figure 2.3F). These results are in line with a previous study that reported on FES substrate recognition.[14] Lastly, a modified PamChip array to measure phosphopeptide binding to the Src homology 2 (SH2) domain of FES^{WT} and FES^{S700C} showed that the introduced mutation did not affect the SH2 binding profile (Figure 2.3G and Supplementary Table 2.2). In short, the DFG-1 residue (S700) in the ATP-binding pocket of FES was identified as an excellent position to mutate into a nucleophilic cysteine, without affecting FES kinase activity, kinetics, substrate recognition and SH2 binding profile.

Design, synthesis and characterization of complementary probes for FES^{S700C}

The reversible ligand TAE684 was used as a starting point to develop a complementary probe for FES^{S700C}. To assess whether the FES^{S700C} was still sensitive to inhibition by TAE684, the protein was incubated with various concentrations of TAE684 and its half maximum inhibitory concentration (expressed as pIC_{50}) was determined. This revealed that TAE684 was a potent inhibitor both on FES^{WT} and FES^{S700C} with pIC_{50} values of 8.1 ± 0.04 and 9.0 ± 0.02, respectively (Table 2.1). According to the co-crystal structure of FES^{WT} with TAE684 (PDB: 4e93) the isopropyl sulfone moiety is in the close proximity of the S700 residue at the DFG-1 position. Therefore, several derivatives of TAE684 were synthesized, in which the R_2-phenyl ring was substituted with an acrylamide group as electrophilic warhead (Scheme 2.1 and Supplementary Scheme 2.1-2.4).

The acrylamide is hypothesized to covalently interact with the engineered cysteine, but not with the serine of the wild-type protein. Since the strategy aims at exclusively inhibiting mutant but not wild-type FES, the piperidine-piperazine group was

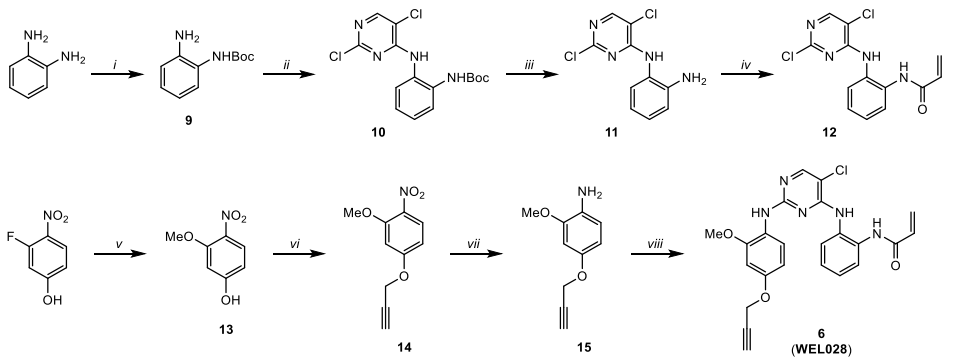

Scheme 2.1 - Synthesis of WEL028. Reagents and conditions: *i*) Boc_2O, THF, rt, 58%. *ii*) 2,4,5-trichloropyrimidine, DIPEA, EtOH, reflux, 92%. *iii*) TFA, DCM, rt, 85%. *iv*) acryloyl chloride, DIPEA, DCM, 0 °C, 85%. *v*) NaOMe, MeOH, 50 °C, 94%. *vi*) propargyl bromide, K_2CO_3, DMF, 60 °C to rt, 88%. *vii*) $SnCl_2$, HCl, 1,4-dioxane, rt, 77%. *viii*) compound **12**, *p*-TSA, isopropanol, reflux, 36%.

removed as it is known to form water-mediated hydrogen bonds with hinge region residues and contribute to ligand affinity.[23] The pIC_{50} values of compound **2**-**6** are listed in Table 2.1 (dose-response curves in Supplementary Figure 2.1B-F). Removal of the piperidine-piperazine group (compound **2**) resulted in a modest reduction in potency on FES^{WT} and FES^{S700C}. Introduction of an acrylamide at the *meta*-position of the phenyl ring (compound **3**) further decreased affinity for FES^{WT}, but also led to significant loss in activity on the FES^{S700C} mutant. Moving the acrylamide to the *ortho*-position resulted in compound **4,** which exhibited excellent potency on FES^{S700C} (pIC_{50} = 8.4 ± 0.03), whereas a major reduction in potency on FES^{WT} (pIC_{50} = 5.7 ± 0.21) was found, resulting in an apparent selectivity window of 238-fold. The acrylamide was substituted for a propionamide (compound **5**) to confirm its important role in binding to FES^{S700C}. In line with the proposed mode of action, compound **5** displayed low inhibitory potency on FES^{S700C}.

Next, a docking study was performed with compound **4** in FES^{S700C} (Figure 2.4A). The binding mode of **4** resembled the original binding pose of TAE684 and could explain the observed structure-activity relationships. Catalytic lysine residue 590 interacts with the amide carbonyl, ideally positioning the warhead on the *ortho*-position, but not on the *meta*-position, to undergo a Michael addition with the engineered cysteine. The binding pose also revealed a suitable position to install an alkyne moiety on the scaffold of compound **4** to develop a two-step chemical probe for target engagement studies. This led to the synthesis of compound **6** (hereafter referred to as WEL028) with an *ortho*-acrylamide and alkyne ligation handle (Scheme 2.1), which displayed a similar potency profile as **4** with strong inhibition of FES^{S700C} (pIC_{50} = 8.4 ± 0.03) but not FES^{WT} (pIC_{50} = 5.0 ± 0.37) (Figure 2.4B and Table 2.1). The mutant-specific inhibition profile was additionally verified using the orthogonal PamChip® microarray assay (Figure 2.4C).

Table 2.1 - Inhibitory potency of synthesized TAE684 derivatives against FES^{WT} and FES^{S700C}. Half maximal inhibitory concentrations (expressed as pIC_{50}) determined on recombinantly expressed FES^{WT} and FES^{S700C} in a TR-FRET assay. Apparent fold selectivity was calculated as IC_{50} on FES^{WT} divided by IC_{50} on FES^{S700C}. Data represent means ± SD (N = 3). ND: not determined. Dose-response curves can be found in Figure 2.4B and Supplementary Figure 2.1).

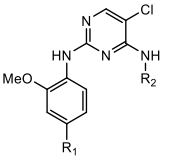

Compound	R_1	R_2	pIC_{50}		Apparent fold selectivity
			FES^{WT}	FES^{S700C}	
1 (**TAE684**)	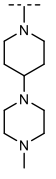	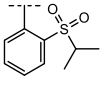	8.1 ± 0.04	9.0 ± 0.02	8.6
2	H	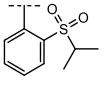	7.3 ± 0.06	7.8 ± 0.04	2.5
3	H	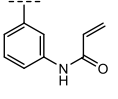	6.5 ± 0.06	6.3 ± 0.06	0.65
4	H	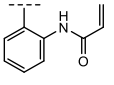	5.7 ± 0.21	8.4 ± 0.03	238
5	H	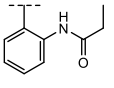	ND	5.2 ± 0.08	ND
6 (**WEL028**)	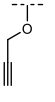	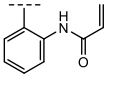	5.0 ± 0.37	8.4 ± 0.03	232

To confirm that WEL028 undergoes a Michael addition to cysteine 700, recombinant FES^{S700C} was incubated with WEL028, digested to peptide fragments with trypsin and subsequently analyzed by LC-MS/MS (Figure 2.4D and Supplementary Figure 2.2). The mass of the expected FES peptide covalently bound to WEL028 was identified, whereas this mass was not present in a vehicle-treated control sample. The parent ion was further analyzed by collision-induced dissociation and the corresponding MS/MS fragmentation pattern showed clear ladders of predicted b and y ions, which confirmed covalent addition of WEL028 to Cys700.

Cys700 is located directly adjacent to the DFG motif, which is highly conserved among kinases and plays an essential role in binding Mg^{2+} ions that coordinate to the phosphates of ATP.[40] A substantial number of kinases also harbors a native cysteine at this

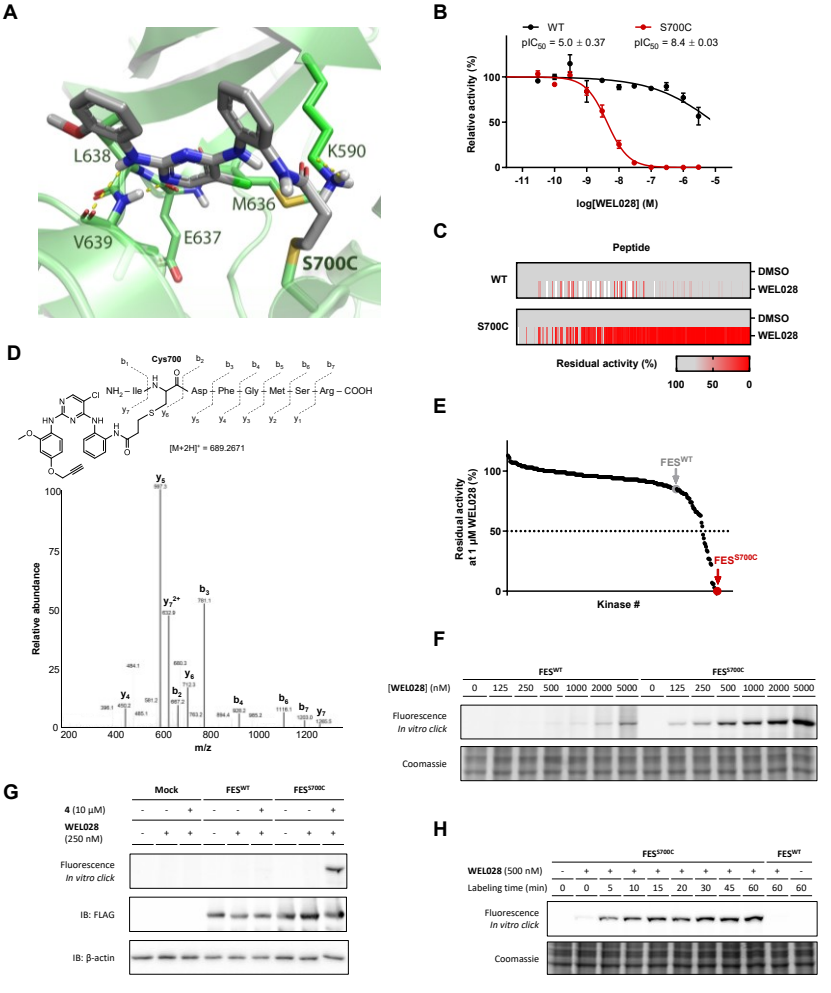

Figure 2.4 – WEL028 is a mutant-specific inhibitor of FES^{S700C} that covalently binds to Cys700. (A) Proposed covalent binding mode of compound **4** to Cys700 in crystal structure of FES (PDB code: 4e93). **(B)** *In vitro* inhibition profile of FES^{WT} and FES^{S700C} by WEL028. Data was obtained using time-resolved FRET assay. **(C)** Inhibition profile of WEL028 (100 nM) on FES^{WT} and FES^{S700C} on individual peptide substrates determined in PamChip® microarray. Signal intensity was normalized to vehicle-treated control. **(D)** MS/MS-based identification of WEL028 covalently bound to Cys700. The precursor ion (m/z [M+2H]$^{2+}$ = 689.2671) was fragmented and signature ions of the WEL028-bound peptide are shown. The precursor ion was not observed in a vehicle-treated control sample. **(E)** Selectivity profile of WEL028 (1 µM, 1 h pre-incubation) on 279 kinases including all kinases with native active site cysteines, visualized as waterfall plot (each data point is an individual kinase). Kinases with <50% inhibition at 1 µM were further profiled in dose-response experiments. Data represent means (N = 2) and were obtained from SelectScreen™ selectivity profiling service except for FES^{S700C}, which was determined in-house. **(F)** Visualization of dose-dependent labeling of full-length FES^{S700C} but not FES^{WT} in HEK293T cell lysate using click chemistry. Lysates were incubated with WEL028 (indicated concentration, 30 min, rt), followed by addition of click mix containing Cy5-azide (2 eq., 30 min, rt). **(G)** Two-step labeling by WEL028 is specific and exclusive for FES^{S700C}. Lysate was incubated with vehicle or compound **4** (10 µM, 30 min, rt), followed by WEL028 (250 nM, 30 min, rt) and click mix containing Cy5-azide (2 eq., 30 min, rt). Protein expression was verified by immunoblot against a C-terminal FLAG-tag and β-actin as loading control. **(H)** Time-dependent labeling of FES^{S700C} by WEL028. Lysates were incubated with WEL028 (500 nM, indicated time, rt) and visualized by click chemistry as in F. Data represent means ± SEM (N = 3).

position, which might have implications for the kinome-wide selectivity of WEL028.[34] The selectivity profile was therefore assessed using the SelectScreen™ screening technology in a panel of 279 wild-type, mammalian kinases including all kinases with a native cysteine residue at any position in the active site. The assays were performed at a single dose of 1 µM with 1 h of pre-incubation to identify the full spectrum of potential off-target kinases. Only 19 of the tested 279 kinases showed >50% inhibition under these conditions, meaning that WEL028 exhibited a >100-fold selectivity window against the residual 260 kinases (93% of tested kinases, Figure 2.4E and Supplementary Figure 2.3). Subsequently, dose-response experiments were performed for kinases showing >50% inhibition in the initial screen (Table 2.2 and Supplementary Figure 2.4). The only off-targets of WEL028 with a pIC_{50} ≤7 were LRRK2 (pIC_{50} = 7.3 ± 0.05) and MKNK2 (pIC_{50} = 7.0 ± 0.06). Importantly, the potency of WEL028 on FES^{S700C} was unmatched by any of the tested kinases, with a minimal 10-fold apparent selectivity window in all cases.

Table 2.2 – Selectivity profile of WEL028. All data (pIC_{50} ± SD, N = 2) were obtained from SelectScreen™ selectivity profiling service except for FES^{S700C}, which was determined in-house. Kinases exhibiting >50% inhibition at 1 µM in an initial screen on 279 kinases (Supplementary Figure 2.3) were selected for dose-response experiments. Assays were performed with 1 h pre-incubation. Indicated molecular weight is based on UniProt database records. Location of native cysteine residues in the kinase active site is indicated if applicable, with nomenclature as previously described.[27] Apparent fold selectivity was calculated as IC_{50} on that kinase divided by IC_{50} on FES^{S700C}. Dose-response curves can be found in Supplementary Figure 2.4.

Kinase	Molecular weight (kDa)	Native cysteine	pIC_{50}	Apparent fold selectivity
AURKA	45.8	None	6.2 ± 0.06	155
BRAF	84.4	Hinge2	7.0 ± 0.06	25
CLK4	57.5	None	5.9 ± 1.3	272
FES^{S700C}	**93.5**	**DFG-1**	**8.4 ± 0.03**	**N/A**
FLT3	112.9	DFG-1	5.5 ± 0.10	718
FLT4 (VEGFR3)	152.8	DFG-1, Hinge2	6.7 ± 0.07	50
KDR (VEGFR2)	151.5	DFG-1, Hinge2	6.2 ± 0.06	153
LRRK2	286.1	None	7.3 ± 0.05	12
MAP2K1 (MEK1)	43.4	DFG-1, GK-1	6.6 ± 0.06	60
MAP2K2 (MEK2)	44.4	DFG-1, GK-1	6.6 ± 0.06	54
MAP2K6 (MEK6)	37.5	DFG-1, GK-1	6.5 ± 0.07	68
MAP3K8 (COT)	52.9	DFG+1	6.6 ± 0.05	57
MAPKAPK5 (PRAK)	54.2	DFG-1	6.3 ± 0.09	112
MKNK2 (MNK2)	51.9	DFG-1	7.0 ± 0.06	23
PDGFRA	122.7	DFG-1, Hinge2	6.1 ± 0.06	184
PTK2 (FAK)	119.2	Hinge2	6.4 ± 0.06	89
ROS1	263.9	None	< 5	> 238
STK33	57.8	Hinge2	6.0 ± 0.58	254
TNK2 (ACK)	114.6	None	6.5 ± 0.26	76

To visualize covalent binding of FES^{S700C} by WEL028, full-length FES^{S700C} was overexpressed in HEK293T cells and cell lysates were incubated with different concentrations of WEL028, followed by *in vitro* conjugation to a Cy5 fluorophore using click chemistry. Dose-dependent labeling at the expected molecular weight of 93 kDa was observed for FES^{S700C} but not FES^{WT} (Figure 2.4F). Pre-incubation with compound **4** completely abolished labeling of FES^{S700C} (Figure 2.4G). Time course experiments revealed that complete labeling was achieved within 15 min incubation and that labeling was stable up to 60 min (Figure 2.4H). In summary, WEL028 was identified as a complementary two-step probe for engineered FES^{S700C} that does not label wild-type FES and is highly selective over other kinases.

Target engagement studies with complementary one-step probe WEL033

Next, a one-step fluorescent probe was synthesized to facilitate visualization of FES^{S700C}: a Cy5-conjugated analog of WEL028 termed WEL033 (Figure 2.5A and Supplementary Scheme 2.5). WEL033 dose-dependently labeled recombinantly expressed full-length FES^{S700C} but not FES^{WT} in HEK293T cell lysate (Figure 2.5B). Interestingly, introduction of a secondary K590E mutation, resulting in a kinase-dead FES mutant that is unable to acquire an active "DFG-in" conformation[17], abolished labeling by WEL033 (Figure 2.5C). This indicates that the Lys590 residue is essential for covalent binding of WEL028 to the FES active site, either directly by coordination of Lys590 to position the acrylamide warhead to undergo covalent addition to Cys700 as predicted by the docking studies (Figure 2.4A), or indirectly by restricted access to the inactive "DFG-out" conformation of FES.

A competitive probe binding assay was then performed to visualize target engagement in lysates with overexpressed full-length FES^{S700C}. Two inhibitors, TAE684 and WEL028, were able to prevent the labeling of FES^{S700C} in a dose-dependent manner (pIC_{50} = 7.6 ± 0.06 and pIC_{50} = 7.9 ± 0.06, respectively; Figure 2.5D, E). A similar dose-dependent profile was observed for **4** and biotin-conjugate WEL034 (Supplementary Figure 2.5). This demonstrates that gel-based ABPP using lysates of cells expressing full-length engineered FES^{S700C} is a valuable orthogonal method to standard biochemical assays using purified, truncated proteins.

The mode of action of TAE684 and WEL028 was then evaluated using time-dependent displacement experiments with these inhibitors (Figure 2.5F, G). After inhibitor incubation at their respective IC_{80} concentrations, labeling of FES^{S700C} activity by WEL033 recovers for TAE684 but not for WEL028, indicating a reversible and irreversible mode of action for these compounds, respectively. In line with these results, inhibitor washout experiments using overnight dialysis also showed irreversible inhibition by WEL028 but not

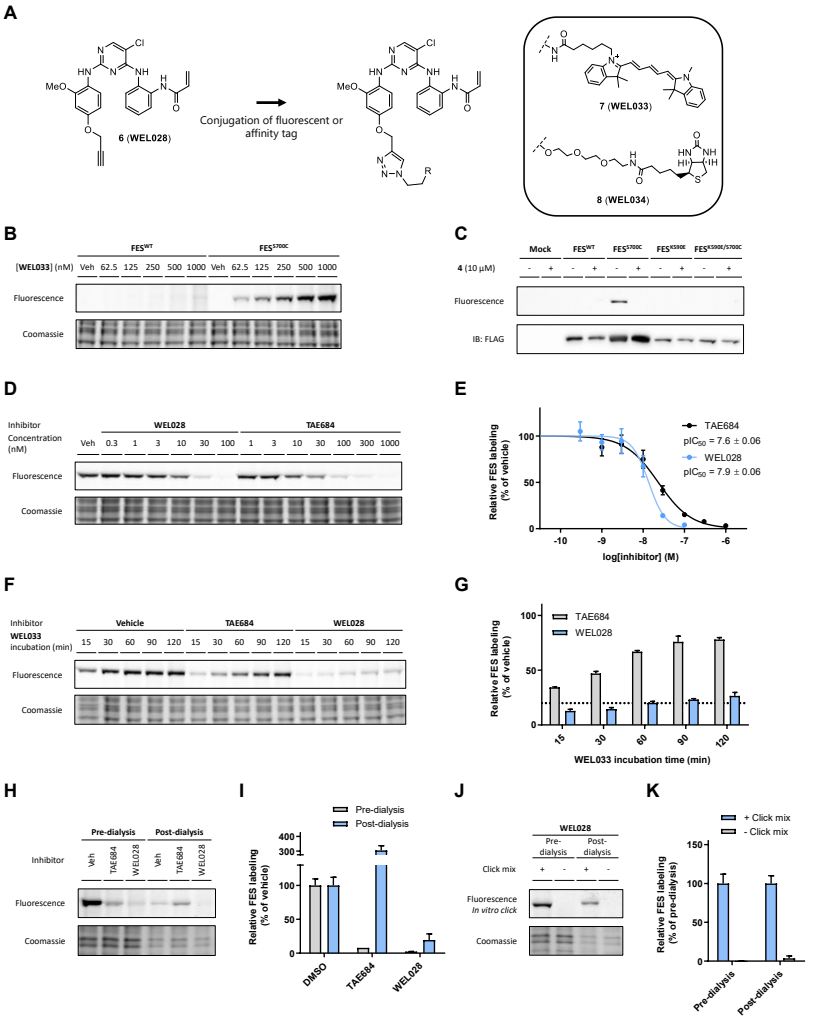

Figure 2.5 - Characterization of one-step probe WEL033 for visualization of FES^{S700C} target engagement. **(A)** Design of one-step probes WEL033 (Cy5-conjugate) and WEL034 (biotin-conjugate) from two-step probe WEL028. **(B)** Dose-dependent labeling of full-length FES^{S700C} but not FES^{WT} by WEL033 (indicated concentration, 30 min, rt) in HEK293T lysate. **(C)** Labeling by WEL033 is specific, exclusive for FES^{S700C} and dependent on catalytic lysine 590. Lysates were incubated with vehicle or **4** (10 µM, 30 min, rt), followed by WEL033 (250 nM, 30 min, rt). Protein expression was verified by immunoblot against a C-terminal FLAG-tag. **(D, E)** Visualization of FES^{S700C} target engagement by WEL028 and TAE684. Lysate was pre-incubated with WEL028 or TAE684 (indicated concentration, 30 min, rt), followed by incubation with probe WEL033 (250 nM, 30 min, rt). Band intensities were normalized to vehicle-treated control. **(F, G)** WEL033 outcompetes TAE684 but not WEL028 binding over time. Lysate was incubated with vehicle, TAE684 or WEL028 at the respective IC_{80}-concentration (20% remaining activity; TAE684: 82 nM, WEL028: 27 nM; 30 min, rt), followed by incubation with WEL033 (1 µM, indicated time, rt). Band intensities were normalized to vehicle-treated control at same time point. **(H, I)** Sustained FES^{S700C} inhibition by WEL028 but not TAE684 after overnight dialysis. Lysates were treated with vehicle, TAE684 or WEL028 as in panel F. Pre-dialysis samples were directly flash-frozen after incubation and residual lysate was dialyzed overnight at 4 °C. Pre- and post-dialysis samples were then labeled by WEL033 (250 nM, 30 min, rt). Band intensities were normalized to vehicle-treated control. **(J, K)** Two-step labeling of WEL028-bound FES^{S700C} before and after dialysis. Samples were processed as in panel H, but conjugated to BODIPY-azide using click chemistry (2 eq., 30 min, rt). Band intensities were normalized to pre-dialysis control. Data represent means ± SEM (N = 3).

TAE684 (Figure 2.5H, I). Direct visualization of the covalent adduct using click chemistry confirmed sustained engagement of FES^{S700C} by WEL028 post-dialysis (Figure 2.5J, K). Of note, the labeling intensity of vehicle-treated control samples was decreased after dialysis, possibly due to protein degradation or aggregation. Interestingly, the labeling intensity TAE684-treated FES^{S700C} post-dialysis was higher than the vehicle-treated control, indicating that this reversible ligand may induce a conformational change that increases protein stability.

Subsequently, it was investigated whether WEL028 could also engage FES^{S700C} in living cells. To this end, HEK293T cells overexpressing FES^{WT} or FES^{S700C} were incubated with various concentrations of WEL028, after which cells were harvested and lysed. WEL028-labeled proteins were then visualized using click chemistry. Dose-dependent labeling of FES^{S700C} was observed (Figure 2.6A), which indicates that WEL028 is cell-permeable and can serve as a two-step probe in living cells. Interestingly, the potency of WEL028 *in situ* (pIC_{50} = 7.6 ± 0.05, Figure 2.6B) is similar to its potency *in vitro* (pIC_{50} = 7.9 ± 0.06, Figure 2.5E), which demonstrates the benefit of an irreversible binding mode with lower susceptibility to high intracellular ATP concentrations.

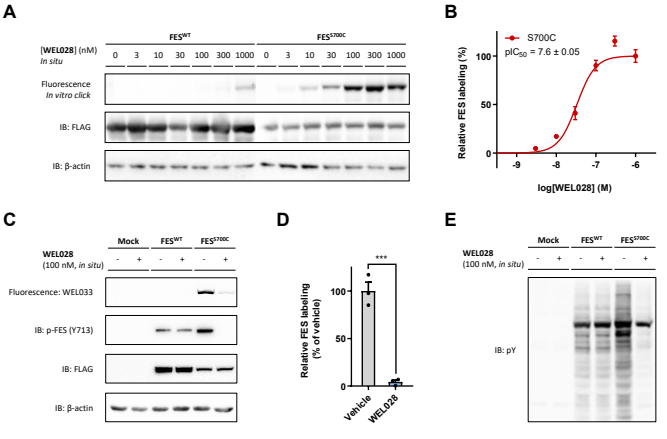

Figure 2.6 – WEL028 engages FES^{S700C} in live cells, blocks FES autophosphorylation and reduces downstream tyrosine phosphorylation. (A, B) WEL028 engages recombinantly expressed FES^{S700C} in live cells. HEK293T cells were transfected with FES^{WT} and FES^{S700C} and 48 h post-transfection, cells were treated with WEL028 (indicated concentration, 1 h, 37 °C). Cells were harvested, lysed and WEL028-labeled proteins were visualized by conjugation to Cy5-azide using click chemistry. Protein expression was verified by immunoblot against a C-terminal FLAG-tag and β-actin served as loading control. Band intensities were normalized to highest concentration. **(C, D)** WEL028 blocks FES^{S700C} but not FES^{WT} autophosphorylation *in situ*. U2OS cells were transfected as in panel A and treated with WEL028 (100 nM, 1 h, 37 °C). Lysates were incubated with WEL033 (250 nM, 30 min, rt) to post-label residual active FES. Autophosphorylation at Y713 was visualized by immunoblot. Band intensities were normalized to vehicle-treated control. **(E)** WEL028 reduces global tyrosine phosphorylation downstream of FES^{S700C} but not FES^{WT}. Samples were processed as in D and tyrosine phosphorylation was visualized by immunoblot using anti-phosphotyrosine antibody (4G10). Data represent means ± SEM (N = 3). Statistical analysis was performed using two-tailed t-test: *** P <0.001.

To determine whether WEL028 also blocked FES-mediated phosphorylation *in situ*, FES^{WT}- or FES^{S700C}-overexpressing cells were incubated with WEL028 (100 nM, 1 h), followed by lysis and visualization of residual FES activity by WEL033 (Figure 2.6C). Under these conditions, WEL028 showed >90% engagement of FES^{S700C} (Figure 2.6D). Autophosphorylation of Y713 on the activation loop of FES is a hallmark for its kinase activity.[14,15,41] Consequently, immunoblot analysis using a phospho-specific antibody for pY713 revealed that WEL028 fully abolished autophosphorylation of FES^{S700C} but not FES^{WT}. Furthermore, a drastic increase in the global phosphotyrosine profile was observed upon overexpression of FES^{WT} or FES^{S700C} (Figure 2.6E), which was almost completely blocked by acute inactivation of FES^{S700C} by WEL028. This indicates that the target engagement as measured by gel-based ABPP assay correlates with the functional activity of FES^{S700C} as determined in the biochemical and immunoblot assays.

Applicability to other kinases

To investigate the broader applicability of this strategy, it was explored whether the complementary probes could also target other kinases than FES in a similar chemical genetic strategy. To this end, a cysteine residue was introduced at the DFG-1 position (S701) of the kinase FER, which together with FES forms a unique kinase subfamily with high structural and functional similarity.[11] FER^{WT} and FER^{S701C} were recombinantly expressed, purified and biochemically characterized and exhibited similar affinity for ATP (K_M = 11 µM for FER^{WT} and K_M = 3.5 µM for FER^{S701C}; Supplementary Figure 2.6A). Profiling the panel of synthesized compounds on FER^{WT} and FER^{S701C} (Supplementary Table 2.3 and Supplementary Figure 2.6B-F) revealed that WEL028 potently targeted mutant but not wild-type FER (pIC_{50} = 6.3 ± 0.36 for FER^{WT}, pIC_{50} = 8.2 ± 0.06 for FER^{S701C}). Moreover, incubation of cell lysates from HEK293T cells overexpressing FER^{S701C} with WEL033 resulted in dose-dependent labeling that was prevented by pre-incubation with inhibitor **4** (Figure 2.7A, B).

In addition, cysteine mutants were generated of two other tyrosine kinases with lower sequence similarity and different amino acids at the DFG-1 position: LYN and PTK2 (resulting in LYN^{A384C} and $PTK2^{G536C}$, respectively). Overexpression of these kinases and incubation with complementary probes exhibited dose-dependent, mutant-specific labeling (Figure 2.7C-F). Interestingly, no labeling was observed for LYN^{A384C} with one-step probe WEL033 (data not shown), which may indicate that the bulky Cy5 fluorophore prohibits active site binding in this particular case. Finally, it was investigated whether PAK4, a kinase belonging to the serine/threonine kinase subgroup, could also be sensitized to the complementary probes in a similar fashion. Strikingly, also this corresponding mutant $PAK4^{S457C}$ but not $PAK4^{WT}$ was dose-dependently labeled by WEL033 (Figure 2.7G, H). In conclusion, these results suggest that the here presented chemical genetic strategy is not exclusively applicable to tyrosine kinases closely related to FES, but can also be employed to visualize target engagement of kinases with lower structural and functional similarity.

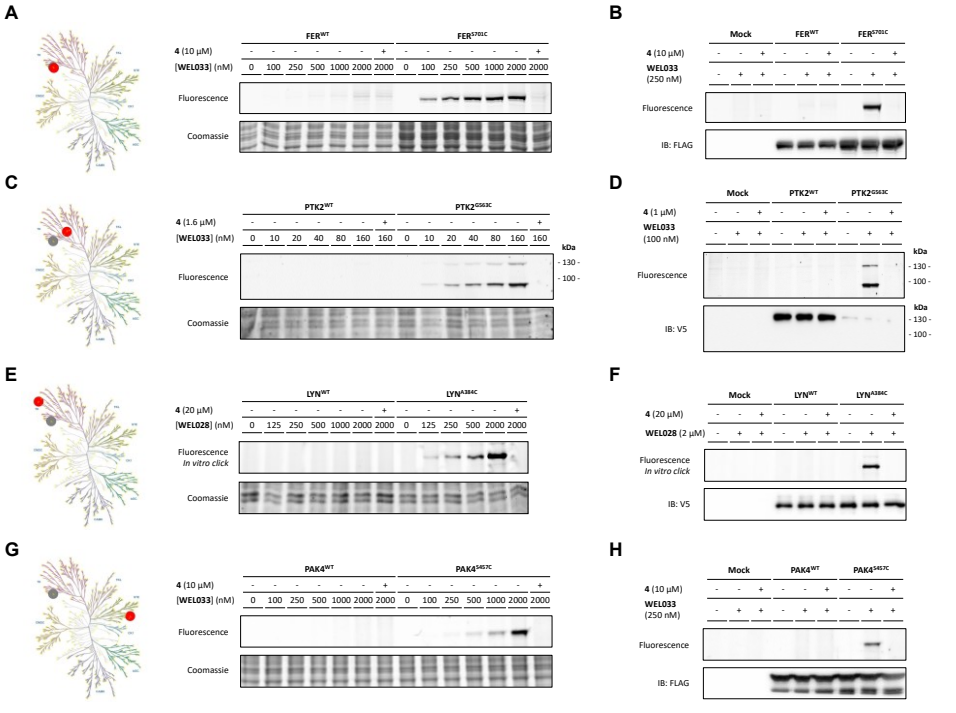

Figure 2.7 - Applicability of chemical genetic strategy on various kinases with DFG-1 residues mutated into cysteine. (A, C, E, G) Dose-dependent labeling of DFG-1 cysteine mutants but not wild-type kinases by complementary probes. Recombinantly expressed kinase (A: FER, C: PTK2, E: LYN, G: PAK4) in HEK293T cell lysate was pre-incubated with vehicle or **4** (indicated concentration, 30 min, rt), followed by incubation with probe (A, C, G: one-step probe WEL033, E: two-step probe WEL028; indicated concentrations, 30 min, rt). For E, samples were then conjugated to Cy5-azide using click chemistry. Homology-based similarity of corresponding kinase (red) to FES (gray) is visualized in kinome tree illustrations. **(B, D, F, H)** Labeling by complementary probes is specific and exclusive for DFG-1 cysteine mutants. Samples were treated as aforementioned, but at optimal probe concentration (indicated, 30 min, rt). Protein expression was verified by immunoblot against a C-terminal FLAG-tag or V5-tag. Of note, PTK2 migrated a two bands of which only the upper band was detected by immunoblot. Kinome illustrations were rendered using KinMap (www.kinhub.org/kinmap), reproduced courtesy of Cell Signaling Technology, Inc. (www.cellsignal.com).

Discussion and conclusion

In this chapter, a novel chemical genetic strategy is presented to study kinase target engagement, combining an engineered, mutant kinase with the design and application of complementary covalent probes. The field of chemical genetics has previously generated tools to aid in kinase target validation[42], such as the "analog-sensitive" *(AS)* technology, where the gatekeeper residue is changed into a less bulky residue, enabling the kinase of interest to accommodate bulky ATP analogs in its active site.[43,44] However, these analogs do not form covalent adducts with the kinase and therefore do not readily allow visualization of target engagement. Furthermore, mutagenesis of gatekeeper residues often results in impaired catalytic activity.[45] In addition, the disadvantageous pharmacokinetic properties of ATP analogs used in the *AS* technology, such as a short *in*

vivo half-life, limit their applicability for target validation studies.[46] The concept of "covalent complementarity" is based on mutagenesis of the gatekeeper[30] or gatekeeper+6[32] residue into a cysteine to function as nucleophile. Although this allows the development of covalent probes and thereby target engagement studies, a second mutation in the active site was required to improve gatekeeper cysteine reactivity or compound selectivity and potency.[30,31] This is particularly challenging when moving to an endogenous model system, since it would involve CRISPR/Cas9 gene editing of two independent point mutations.

Importantly, the introduced nucleophilic cysteine needs to be functionally silent, *i.e.* it should not affect catalytic activity and substrate binding. Site-directed mutagenesis of the DFG-1 position into a cysteine fulfilled this criterion. FES^{S700C} retained full catalytic activity and exhibited an identical substrate and SH2 binding profile as FES^{WT}. FES^{S700C} showed a minor increase in ATP binding affinity, but this difference in K_M is unlikely to have any consequences at physiologically relevant ATP concentrations, which are typically in the millimolar range.[34] Although nearly 10% of all known kinases have a native DFG-1 cysteine residue, many kinases harboring a DFG-1 cysteine showed limited or no inhibition by WEL028 (Table 2.2, Supplementary Figure 2.3 and 2.4), suggesting that the choice of the chemical scaffold constitutes an additional selectivity filter. An acrylamide group was selected as the electrophile to react with the intended cysteine, since it exhibits sufficient reactivity towards cysteines only when appropriately positioned for a Michael addition reaction and has limited reactivity to other intracellular nucleophiles.[47] This may additionally prevent non-specific interactions with targets outside of the kinase cysteinome. Given the favorable selectivity profile and cellular permeability of WEL028, the diaminopyrimidine scaffold is a useful addition to the toolbox of covalent complementary probes applied in chemical genetic strategies, which previously consisted of mainly quinazolines and pyrazolopyrimidines.[30,32]

The presented chemical genetic strategy is not limited to FES, but can be applied to other kinases, either structurally related (FER) or more distinct (LYN, PTK2 and PAK4). Complementary probes dose-dependently labeled the corresponding DFG-1 cysteine mutants (Figure 2.7), whereas the kinome selectivity screen (Supplementary Figure 2.3) indicated that wild-type FER, LYN, PTK2 and PAK4 are not potently targeted by WEL028 (pIC_{50} <6 for FER, LYN and PAK4, pIC_{50} = 6.4 ± 0.06 for PTK2). For follow-up target validation studies, however, more thorough biochemical profiling is necessary to establish the selectivity of WEL028 for the mutant over the wild-type kinase of interest, which was in this study only performed for FER (Supplementary Table 2.3). Nevertheless, the selectivity acquired by combining DFG-1 cysteine mutants and a complementary probe enables acute, pharmacological inhibition without the need for extensive hit optimization programs to identify compounds of adequate potency and selectivity for each kinase individually.

In conclusion, the DFG-1 residue in the kinase active site was identified as an excellent position for mutagenesis into a reactive cysteine without affecting kinase function. Complementary, covalent probes WEL028 and WEL033 allow for visualization of target engagement *in vitro* as well as in living cells. Additionally, this chemical genetic strategy can be applied to various kinases in different subfamilies. The favorable selectivity profile of WEL028 makes it a useful tool for acute inactivation of kinase activity *in situ*, especially in combination with functional assays to provide insight in kinase function. This could prove especially useful for kinases with poorly characterized substrates or for kinases with limited availability of selective ligands. It is thus envisioned that the presented methodology could provide powerful tools to visualize target engagement and to study poorly characterized kinases, thereby aiding in their validation as therapeutic target.

Acknowledgments

Riet Hilhorst, Tim van den Hooven and Rob Ruijtenbeek are kindly acknowledged for microarray measurements and helpful discussions, Nienke M. Prins, Jessica Schlachter and Joost. A. P. M. Wijnakker for cloning and expression of constructs, Bogdan I. Florea for mass spectrometry analysis, Eelke B. Lenselink for docking studies and Hans den Dulk for valuable general advice. The Cloning & Purification Facility (Geri F. Moolenaar and Nora Goosen) and Hans van den Elst are acknowledged for technical support.

Experimental procedures - Biochemistry

General

All chemicals were purchased at Sigma Aldrich, unless stated otherwise. DNA oligos were purchased at Sigma Aldrich or Integrated DNA Technologies and sequences can be found in Supplementary Table 2.1. Cloning reagents were from Thermo Fisher. TAE684 was purchased at Selleckchem. Cy5-azide and BODIPY-azide were previously synthesized in-house and characterized by NMR and LC-MS.[48] All cell culture disposables were from Sarstedt. Bacterial and mammalian protease inhibitor cocktails were obtained from Amresco.

Cloning

Full-length human cDNA encoding FES and PAK4 was obtained from Source Bioscience. pDONR223-constructs with full-length human cDNA of FER, LYN and PTK2 were a gift from William Hahn & David Root (Addgene Human Kinase ORF Collection). For bacterial expression constructs, human FES cDNA encoding residues 448-822 (protein MW = 45.8 kDa) or human FER cDNA encoding residues 448-820 (protein MW = 46.2 kDa) was amplified by PCR and cloned into expression vector pET1a in frame with an N-terminal His_6-tag and Tobacco Etch Virus (TEV) recognition site. Eukaryotic expression constructs of FES, FER and PAK4 were generated by PCR amplification and restriction/ligation cloning into a pcDNA3.1 vector, in frame with a C-terminal FLAG-tag. Eukaryotic expression constructs of LYN and PTK2 were generated using Gateway™ recombinational cloning into a pcDest40 vector, in frame with a C-terminal V5-tag, according to recommended procedures (Thermo Fisher). Point mutations were introduced by site-directed mutagenesis and all plasmids were isolated from transformed XL10-Gold competent cells (prepared using *E. coli* transformation buffer set; Zymo Research) using plasmid isolation kits following the supplier's protocol (Qiagen). All sequences were verified by Sanger sequencing (Macrogen).

Supplementary Table 2.1 – List of oligonucleotide sequences.

ID	Name	Sequence
P1	FES_SH2-KD_forw	AGGGCGCCATGGGGATTCCGGAGGTGCAGAAGC
P2	FES_SH2-KD_rev	CACTCGAGCACCGCGGCCGCTTACCGATGCCGCTTTCGGAT
P3	FES_I567C_forw	GTGTTGGGTGAGCAGTGTGGACGGGGGAACTTT
P4	FES_G570C_forw	GAGCAGATTGGACGGTGCAACTTTGGCGAAGTG
P5	FES_V575C_forw	GGGAACTTTGGCGAATGCTTCAGCGGACGCCTG
P6	FES_L638C_forw	TACATCGTCATGGAGTGTGTGCAGGGGGGCGAC
P7	FES_G642C_forw	GAGCTTGTGCAGGGGTGCGACTTCCTGACCTTC
P8	FES_T646C_forw	GGGGGCGACTTCCTGTGCTTCCTCCGCACGGAG
P9	FES_N688C_forw	GACCTGGCTGCTCGGTGCTGCCTGGTGACAGAG
P10	FES_L690C_forw	GCTGCTCGGAACTGCTGCGTGACAGAGAAGAAT
P11	FES_S700C_forw	AATGTCCTGAAGATCTGTGACTTTGGGATGTCC
P12	FES_forw	CTTAAGCTTTGGTACCGCCGCCACCATGGGCTTCTCTTCTGAGC
P13	FES_rev	CATTCTAGATCACTCGAGACCGGTCCGATGCCGCTTTCGGAT
P14	FES_K590E_forw	ACCCTGGTGGCGGTGGAGTCTTGTCGAGAGACG
P15	FES_K590E_rev	CGTCTCTCGACAAGACTCCACCGCCACCAGGGT
P16	FER_SH2-KD_forw	CGTCTCCCATGATCTCCATCAGTGAGAAGCCTT
P17	FER_SH2-KD_rev	CACCGCGGCCGCTTATGTGAGTTTTCTCTTGAT
P18	FER_S701C_forw	AATGTTCTGAAAATCTGTGACTTTGGAATGT
P19	FER_S701C_rev	ACATTCCAAAGTCACAGATTTTCAGAACATT
P20	FER_forw	AGCCGTCTCGGTACCGCCGCCACCATGGGGTTTGGGAGTGACC
P21	FER_rev	CATTCTAGATCACTCGAGACCGGTTGTGAGTTTTCTCTTGA
P22	LYN_A384C_forw	GTCACTCATGTGCAAGATCTGTGATTTTGGCCTTGCT
P23	LYN_A384C_rev	AGCAAGGCCAAAATCACAGATCTTGCACATGAGTGAC
P24	PTK2_G563C_forw	GATTGTGTAAAATTATGCGACTTTGGTCTCTCCCGATATATGGAA
P25	PTK2_G563C_rev	TTCCATATATCGGGAGAGACCAAAGTCGCATAATTTTACACAATC
P26	PAK4_forw	CTTAAGCTTTGGTACCGCCGCCACCATGTTTGGGAAGAGGAAGAA
P27	PAK4_rev	CATTCTAGATCACTCGAGACCGGTTCTGGTGCGGTTCTGGCGCA
P28	PAK4_S457C_forw	GGCAGGGTGAAGCTGTGTGACTTTGGGTTCTGC
P29	PAK4_S457C_rev	GCAGAACCCAAAGTCACACAGCTTCACCCTGCC

Protein expression and purification

Bacterial expression constructs were transformed into *E. coli* BL21(DE3) co-transformed with a pCDFDuet-1 vector encoding *Yersinia* phosphatase YopH (kindly provided by prof. dr. Kuriyan).[35] Cells were grown in Luria Broth (LB) medium containing 50 µg/mL kanamycin and 50 µg/mL streptomycin at 37 °C to an OD_{600} of 0.4. The cultures were cooled on ice and protein expression was induced by addition of isopropyl-β-D-thiogalactopyranoside (IPTG, 50 µM; 16 h, 18 °C, 180 rpm). Cultures (typically 10 mL per mutant) were centrifuged (1000 *g*, 10 min, 4 °C) and washed with 1 mL physiological salt solution (0.9% (w/v) NaCl). The pellet was then resuspended in 400 µL lysis buffer (100 mM NaH_2PO_4 pH 8.0, 500 mM NaCl, 10% glycerol, 0.5 mM tris(2-carboxyethyl)phosphine (TCEP), 20 mM imidazole, 1 x bacterial protease inhibitor cocktail) and cells were lysed by sonication on ice (15 cycles of 4'' on, 9.9'' off at 25% maximum amplitude; Vibra Cell (Sonics)). $MgCl_2$ and OmniCleave (Epicentre) were added to final concentrations of 10 mM and 125 U/mL respectively, and lysates were

incubated for 10 min at rt. Meanwhile, 200 µL Nickel Magnetic Beads (BiMake) were homogenized by vortexing and washed in lysis buffer (3 x 200 µL) using a magnetic separator. Lysate was added to beads and incubated for 1 h at 4 °C with vigorous shaking. Beads were then washed with lysis buffer containing 75 mM imidazole (3 x 400 µL), after which the beads were transferred to a clean Eppendorf tube. Protein was phosphorylated on beads by addition of autophosphorylation buffer (50 mM HEPES pH 7.5, 500 mM NaCl, 5% glycerol, 10 mM dithiothreitol (DTT), 10 mM Na_3VO_4, 2 mM $(NH_4)_2SO_4$, 10 mM $MgCl_2$, 5 mM $MnCl_2$, 2 mM ATP) and vigorous shaking for 2 h at rt. Beads were subsequently washed with lysis buffer containing 20 mM imidazole (3 x 400 µL), after which the protein was eluted in lysis buffer containing 250 mM imidazole (2 x 200 µL). The elution fractions were combined, applied onto a 10 kDa cutoff centrifugal filter unit (Amicon) and centrifuged (14,000 *g*, 10 min, 4 °C). The retentate was reconstituted in 100 µL protein storage buffer (10 mM HEPES pH 7.5, 500 mM NaCl, 5% glycerol, 10 mM DTT), aliquoted and stored at -80 °C. Protein concentration was measured using Qubit fluorometric quantitation (Thermo Fisher) and protein purity was monitored by SDS-PAGE and Coomassie staining.

In vitro TR-FRET kinase assay

Assays were performed in white ProxiPlate-384 Plus™ 384-well microplates (Perkin Elmer). Incubation steps were performed at 21 °C in kinase reaction buffer (50 mM HEPES pH 7.5, 150 mM NaCl, 10 mM $MgCl_2$, 1 mM EGTA, 2 mM DTT, 0.01% Tween-20). Purified proteins were diluted in kinase reaction buffer prior to use. All measurements were performed in triplicate.

Plates were read on a TECAN Infinite M1000 Pro plate reader, using fluorescence top reading settings (λ_{ex} = 320/20 nm, $\lambda_{em,donor}$ = 615/10 nm, $\lambda_{em,acceptor}$ = 665/10 nm, 100 µs integration time, 50 µs lag time). Emission ratios were calculated as fluorescence of acceptor / fluorescence of donor. Z′-factors were determined for each individual assay plate as $Z' = 1 - 3(\sigma_{pc} + \sigma_{nc})/(\mu_{pc} - \mu_{nc})$, with σ = standard deviation and µ = mean of measured replicates, wild-type or untreated samples as positive control (pc) and samples incubated with no ATP as negative control (nc). All plates met the requirement of Z′ >0.7. Emission ratios were corrected for background signal of samples incubated with no ATP. Corrected ratios were averaged and normalized to wild-type or untreated signal as 100% reference.

For relative activity determination of mutants, purified wild-type or mutant FES (12.5 ng per well) or FER (5 ng per well) was incubated with 50 nM U*Light*-TK peptide (Perkin Elmer) and 100 µM ATP for 60 min at 21 °C in a total volume of 10 µL. The reaction was quenched by addition of 10 µL development solution (20 mM EDTA, 4 nM Europium-anti-phosphotyrosine antibody (PT66, Perkin Elmer) and incubated for 60 min before fluorescence was measured.

For K_M determinations, assay was performed as described above, but with variable ATP concentrations in a dilution series of 1 mM to 100 nM. For IC_{50} determinations, serial dilutions of inhibitor were prepared in DMSO, followed by further dilution in kinase reaction buffer. The inhibitors were premixed with peptide and ATP (5 µM final concentration, unless indicated otherwise), after which wild-type or mutant kinase was added to initiate the reaction. The final DMSO concentration during the reaction was 1%. K_M and IC_{50} curves were fitted using GraphPad Prism® 7 (GraphPad Software Inc.).

PamChip® microarray assay

Kinase activity assay

Kinase activity profiles were determined using the PamChip® 12 protein tyrosine (PTK) peptide microarray system (PamGene International B.V.) according to the instructions of the manufacturer, essentially as described[49] with the exception that arrays were blocked with 2% BSA and the assay buffer contained EDTA instead of EGTA. Sample input was 0.25 ng purified FES (wild-type or S700C) per array and [ATP] = 400 µM. For arrays with inhibitor, recombinant FES was pre-incubated in assay mix without ATP with vehicle or WEL028 (100 nM, 30 min, on ice, 2% final DMSO concentration).

SH2 domain binding assay

PamChip® protein tyrosine kinase (PTK) arrays were blocked by pumping a 2% BSA solution up and down through the array (30 µL, 15 min, 2 cycles/min). After three washing steps, the arrays were pre-phosphorylated by incubation with 1.5 pmol of (His_6-tagged) JAK2 catalytic domain for 60 cycles in kinase assay buffer with 0.01% BSA. After 3 washing steps, the arrays were incubated with 0.75 µg of FES (wild-type or S700C) in PBS/0.1% Tween-20 supplemented with 0.01% BSA. Incubations without FES served as negative control. After 3 washing steps, binding of FES was visualized by incubation with Alexa Fluor 488 labeled anti-penta-His antibody (Qiagen, #1019199), 1 µL per array, in PBS/0.01% Tween-20. Peptide phosphorylation of JAK2 was detected with the same anti p-Tyr antibody as used in the PTK activity assay. After incubation for 30 min (2 cycles/min), arrays were washed, and images taken at different exposure times.

Data analysis and quality control

Data quantification of the images at all exposure times and reaction times and visualization of the data were performed using BioNavigator software (PamGene International B.V.). Post-wash signals (local background subtracted) were used. After signal quantification and integration of exposure times, signals were log2-transformed for visualization. Peptides with no ATP-dependent signal were excluded from analysis. Identification of peptides that were significantly different between conditions was performed using a Mixed Model statistical analysis. Substrate consensus motif was generated using Enologos (http://www.benoslab.pitt.edu).

Selectivity profiling

Selectivity profiling assays were performed by the Invitrogen SelectScreen™ Services. A complete list of tested kinases can be found in Supplementary Figure 2.3, detailed assay procedures are described in SelectScreen Assay Conditions documents located at www.invitrogen.com/kinaseprofiling. All kinases were pre-incubated for 1 h at indicated concentrations of inhibitor. The concentration of ATP was selected to be equal to the K_M, unless indicated otherwise. An initial screen was performed on 279 kinases at single dose of 1 µM. All available kinases with native cysteine residues in the active site were included in this panel. Kinases showing >50% inhibition at 1 µM were further profiled in dose-response experiments in a 10-point dilution series of 10 µM to 0.5 nM.

Docking studies

All structure-based modeling was performed in Schrödinger Suite 2017-2 (Schrödinger). The docking of compound **4** was based on the crystal structure of FES co-crystallized with TAE684 (PDB: 4e93)[23], which was prepared by the protein preparation wizard. Prior to docking, the Ser700 residue was manually changed into a cysteine. Subsequently, compound **4** was aligned to TAE684 on the basis of the diaminopyrimidine (both ligands share the same kinase/hinge binding moiety). This pose was optimized using an exhaustive hierarchical optimization procedure available in Prime.[50] The acrylamide warhead was found in proximity of Cys700 and the ligand was then covalently attached to this residue, followed by another round of hierarchical optimization.[50] Figures were rendered using PyMOL Molecular Graphics System (Schrödinger).

MS identification of covalent inhibitor-peptide adduct

Purified FES^{S700C} (1.2 µg in 38 µL) was treated with vehicle or WEL028 (2 µL of 20x concentrated stock in DMSO, 1 µM final concentration) for 30 min at rt. The reaction was quenched by addition of 3x Laemmli buffer (20 µL), incubated for 5 min at 95 °C and sample (400 ng, 20 µL) was resolved by SDS-PAGE on a 10% polyacrylamide gel (200 V, 60 min). Gel was stained using Coomassie Brilliant Blue R-250, bands were cut out of gel into small blocks and then destained in 500 µL of 50% MeOH in 100 mM NH_4HCO_3 pH 8.0 for 10 min at rt. Acetonitrile (500 µL) was added for gel blocks dehydration, after which gel blocks were digested with sequencing-grade trypsin (Promega) in 250 µL trypsin buffer (100 mM Tris pH 7.5, 100 mM NaCl, 1 mM $CaCl_2$, 10% acetonitrile) overnight at 37 °C with vigorous shaking. The pH was adjusted with formic acid to pH 3, after which the sample was diluted in extraction solution

(65% acetonitrile/35% MilliQ) and concentrated in a SpeedVac concentrator. Samples were subsequently desalted using stage tips with C_{18} material and processed as previously described.[51]

Tryptic peptides were analyzed on a Surveyor nano-LC system (Thermo) hyphenated to a LTQ-Orbitrap mass spectrometer (Thermo) as previously described.[52] General mass spectrometric conditions were: electrospray voltage of 1.8 kV, no sheath and auxiliary gas flow, ion transfer tube temperature 150 °C, capillary voltage 41 V, tube lens voltage 150 V. Internal mass calibration was performed with polydimethylcyclosiloxane (m/z = 445.12002) and dioctyl phthalate ions (m/z = 391.28429) as lock mass. Samples of 10 µl were separated via a trap-elute setup at 250 nL/min flow and analyzed by data-dependent acquisition of one full scan/ top 3 method. For shotgun proteomics, fragmented precursor ions measured twice within 10 s were dynamically excluded for 60 s and ions with z <2 or unassigned charges were not analyzed. Peptide ID was determined with the Mascot search engine. A parent ion list of the m/z ratios of the active-site peptides was compiled and used for LC-MS/MS analysis in a data-dependent protocol. The parent ion was electrostatically isolated in the ion trap of the LTQ and fragmented by MS/MS. Data from MS/MS experiments were validated manually.

Inhibitor washout by dialysis

FES^{S700C}-overexpressing HEK293T lysate (396 µL, 1.43 mg/mL) was incubated with vehicle, TAE684 or WEL028 (4 µL of 100x concentrated stock in DMSO) at final concentrations corresponding to their respective IC_{80} values (TAE684: 225 nM, WEL028: 231 nM) for 30 min at rt. One fraction (200 µL) of the sample was immediately flash-frozen and stored at -80 °C until use. The remaining sample was transferred to a dialysis cassette (Slide-A-Lyzer™ Dialysis Cassette, 7K MWCO, 0.5 mL; Thermo Fisher), followed by dialysis in 200 mL PBS overnight at 4 °C. Pre- and post-dialysis samples were then incubated with probe WEL033 or conjugated to BODIPY-N_3 by CuAAC as aforementioned.

Cell culture

General cell culture

Cell lines were purchased at ATCC and were tested on regular basis for mycoplasma contamination. Cultures were discarded after 2-3 months of use. HEK293T (human embryonic kidney) and U2OS (human osteosarcoma) cells were cultured at 37 °C under 7% CO_2 in DMEM containing phenol red, stable glutamine, 10% (v/v) heat-inactivated newborn calf serum (Seradigm), penicillin and streptomycin (200 µg/mL each; Duchefa). Medium was refreshed every 2-3 days and cells were passaged two times a week at 80-90% confluence. Cell viability was assessed by Trypan Blue exclusion and quantification using a TC20™ Automated Cell Counter (Bio-Rad).

Transfection

One day prior to transfection, HEK293T or U2OS cells were transferred from confluent 10 cm dishes to 15 cm dishes. Before transfection, medium was refreshed (13 mL). A 3:1 (m/m) mixture of polyethyleneimine (PEI; 60 µg/dish) and plasmid DNA (20 µg/dish) was prepared in serum-free medium and incubated for 15 min at rt. The mixture was then dropwisely added to the cells, after which the cells were grown to confluence in 72 h. Cells were then harvested by suspension in PBS, followed by centrifugation for 5 min at 200 *g*. Cell pellets were flash-frozen in liquid nitrogen and stored at -80 °C until sample preparation.

Inhibitor treatment in live cells

The term *in situ* is used to designate experiments in which live cell cultures are treated with inhibitor, whereas the term *in vitro* refers to experiments in which the inhibitor is incubated with cell lysates. Compounds were diluted in growth medium from a 1000x concentrated stock solution in DMSO. For *in situ* assays on live transfected cells, cells were transfected prior to treatment as described above. After 48 h, cells were treated with compound for 1 h. Cells were collected by suspension in PBS and

centrifuged (1000 *g*, 5 min, rt). Pellets were flash-frozen in liquid nitrogen and stored at -80 °C until use.

Preparation of cell lysates

Pellets were thawed on ice and suspended in lysis buffer (50 mM HEPES pH 7.2, 150 mM NaCl, 1 mM $MgCl_2$, 0.1% (w/v) Triton X-100, 2 mM Na_3VO_4, 20 mM NaF, 1 x mammalian protease inhibitor cocktail, 25 U/mL benzonase). Cells were lysed by sonication on ice (15 cycles of 4'' on, 9.9'' off at 25% maximum amplitude). Protein concentration was determined using Quick Start™ Bradford Protein Assay (Bio-Rad) and diluted to appropriate concentration in dilution buffer (50 mM HEPES pH 7.2, 150 mM NaCl). Lysates were aliquoted, flash-frozen and stored at -80 °C until use.

Probe labeling experiments

One-step labeling

For *in vitro* inhibition experiments, cell lysate (14 µL) was pre-incubated with inhibitor (0.5 µL, 29x concentrated stock in DMSO, 30 min, rt), followed by incubation with WEL033 (0.5 µL, 30x concentrated stock in DMSO, 30 min, rt). For *in situ* inhibition experiments, treated cell lysate (14.5 µL) was directly incubated with WEL033 (0.5 µL, 30x concentrated stock in DMSO, 30 min, rt). Final concentrations of inhibitors and/or WEL033 are indicated in the main text and figure legends. Reactions were quenched with 4x Laemmli buffer (5 µL, final concentrations 60 mM Tris pH 6.8, 2% (w/v) SDS, 10% (v/v) glycerol, 5% (v/v) β-mercaptoethanol, 0.01% (v/v) bromophenol blue) and boiled for 5 min at 95 °C. Samples were resolved by SDS-PAGE on a 10% polyacrylamide gel (180 V, 75 min). Gels were scanned using Cy3 and Cy5 multichannel settings (605/50 and 695/55 filters, respectively; ChemiDoc™ MP System, Bio-Rad). Fluorescence intensity was corrected for protein loading determined by Coomassie Brilliant Blue R-250 staining and quantified with Image Lab (Bio-Rad). IC_{50} curves were fitted with Graphpad Prism® 7 (Graphpad Software Inc.).

Two-step labeling

For *in vitro* experiments, cell lysate (12 µL) was pre-incubated with inhibitor (0.5 µL, 25x concentrated stock in DMSO, 30 min, rt), followed by incubation with WEL028 (0.5 µL, 26x concentrated stock in DMSO, 30 min, rt). Meanwhile, "click mix" was prepared freshly by combining $CuSO_4$ (1 µL of 15 mM stock), sodium ascorbate (0.6 µL of 150 mM stock), THPTA (0.2 µL of 15 mM stock) and fluorophore-azide (0.2 µL of 150x concentrated stock in DMSO, 2 eq.). Click mix was added to the reaction, followed by incubation for 30 min at rt, after which the reaction was quenched and further processed as described above. For *in situ* inhibition experiments, WEL028-treated cells were lysed and directly incubated with click mix.

Immunoblot

Samples were resolved by SDS-PAGE as described above, but transferred to 0.2 µm polyvinylidene difluoride membranes by Trans-Blot Turbo™ Transfer system (Bio-Rad) directly after fluorescence scanning. Membranes were washed with TBS (50 mM Tris pH 7.5, 150 mM NaCl) and blocked with 5% milk in TBS-T (50 mM Tris pH 7.5, 150 mM NaCl, 0.05% Tween-20) for 1 h at rt.

Membranes were then incubated with either primary antibody in 5% milk in TBS-T (FLAG, V5, β-actin; o/n at 4 °C) or washed three times with TBS-T and incubated with primary antibody in 5% BSA in TBS-T (other antibodies, o/n at 4 °C). Membranes were washed three times with TBS-T, incubated with matching secondary antibody in 5% milk in TBS-T (1 h at rt) and then washed three times with TBS-T and once with TBS. Luminol development solution (10 mL of 1.4 mM luminol in 100 mM Tris pH 8.8 + 100 µL of 6.7 mM *p*-coumaric acid in DMSO + 3 µL of 30% (v/v) H_2O_2) was added and chemiluminescence was detected on ChemiDoc™ MP System.

Primary antibodies: monoclonal mouse anti-FLAG M2 (1:5000, Sigma Aldrich, F3156), monoclonal mouse anti-β-actin (1:1000, Abcam, ab8227), monoclonal mouse anti-V5 (1:5000, Thermo Fisher,

R960-25), streptavidin-HRP (1:2000, Thermo Fisher, N100), polyclonal rabbit anti-phospho-FES Tyr713 (1:1000, Thermo Fisher, PA5-64504), monoclonal mouse anti-phosphotyrosine (4G10, 1:1000, Merck Millipore, 05-321). Secondary antibodies: goat anti-mouse-HRP (1:5000, Santa Cruz, sc-2005), goat anti-rabbit-HRP (1:5000, Santa Cruz, sc-2030).

Statistical analysis

All statistical measures and methods are included in the respective figure or table captions. In brief: all replicates represent biological replicates and all data represent means ± SEM, unless indicated otherwise. Statistical significance was determined using Student's *t*-tests (two-tailed, unpaired) or ANOVA with Holm-Sidak's multiple comparisons correction. *** $P < 0.001$; ** $P < 0.01$; * $P < 0.05$; NS if $P > 0.05$. All statistical analyses were conducted using GraphPad Prism® 7 or Microsoft Excel.

Experimental procedures - Chemistry

General information

All reactions were performed using oven- or flame-dried glassware and dry solvents. Reagents were purchased from Sigma-Aldrich, Acros, and Merck and used without further purification unless noted otherwise. All moisture sensitive reactions were performed under an argon atmosphere. ^{1}H and ^{13}C NMR spectra were recorded on a Bruker AV 400 MHz spectrometer at 400.2 (^{1}H) and 100.6 (^{13}C) MHz or on a Bruker DMX-600 spectrometer at 600 (^{1}H) and 151 (^{13}C) MHz using $CDCl_3$, DMSO-*d6* or MeOD as solvent. Chemical shift values are reported in ppm with tetramethylsilane or solvent resonance as the internal standard ($CDCl_3$: δ 7.26 for ^{1}H, δ 77.16 for ^{13}C; DMSO-*d6*, δ 2.50 for ^{1}H, δ 39.52 for ^{13}C; MeOD: δ 3.31 for ^{1}H, δ 49.00 for ^{13}C). Data are reported as follows: chemical shifts (δ), multiplicity (s = singlet, d = doublet, dd = double doublet, td = triple doublet, t = triplet, q = quartet, br = broad, m = multiplet), coupling constants *J* (Hz), and integration. HPLC purification was performed on a preparative LC-MS system (Agilent 1200 serie) with an Agilent 6130 Quadruple MS detector. High-resolution mass spectra were recorded on a Thermo Scientific LTQ Orbitrap XL. Compound purity (> 95% unless stated otherwise) was determined by liquid chromatography on a Finnigan Surveyor LC-MS system, equipped with a C18 column. Flash chromatography was performed using SiliCycle silica gel type SiliaFlash P60 (230−400 mesh). TLC analysis was performed on Merck silica gel 60/Kieselguhr F254, 0.25 mm. Compounds were visualized using $KMnO_4$ stain (K_2CO_3 (40 g), $KMnO_4$ (6 g) in water (600 mL)) or ninhydrin stain (ninhydrin (1.5 g) in *n*-butanol (100 mL) and 3 mL acetic acid).

Synthesis of tert-butyl (2-aminophenyl)carbamate (9)

To a solution of *o*-phenylenediamine (2.19 g, 20.2 mmol) in THF (20 mL) was dropwisely added a solution of $(Boc)_2O$ (4.45 g, 20.4 mmol) in THF (5 mL). The reaction mixture was stirred at rt for 16 h, after which the mixture was concentrated under reduced pressure and the residue was taken up in a cold mixture of EtOAc/Petroleum ether (1:4 ratio, 15 mL), causing the product to precipitate. The precipitate was collected by filtration and dried to yield the title compound (2.43 g, 11.7 mmol, 58%). ^{1}H NMR (400 MHz, $CDCl_3$): δ 7.28 (s, 1H), 7.00 (td, *J* = 7.6, 1.5 Hz, 1H), 6.82 – 6.74 (m, 2H), 6.28 (s, 1H), 3.55 (s, 2H), 1.51 (s, 9H). ^{13}C NMR (101 MHz, $CDCl_3$): δ 154.0, 140.0, 126.3, 124.9, 120.5, 119.7, 117.7, 117.0, 80.6, 28.5, 28.4. Spectroscopic data are in accordance with those reported in literature.[53]

Synthesis of tert-butyl (2-((2,5-dichloropyrimidin-4-yl)amino)phenyl)carbamate (10)

2,4,5-Trichloropyrimidine (1.18 g, 6.43 mmol) and DIPEA (1.68 g, 13.0 mmol) were dissolved in EtOH (25 mL). To the stirring solution was added compound **9** (1.35 g, 6.48 mmol), after which the reaction mixture was heated at reflux for 16 h. After TLC indicated depletion of starting material, the mixture was allowed to cool to rt and subsequently triturated with cold H_2O (20 mL), causing precipitation of the product. The precipitate was collected by vacuum filtration and dried to yield the title compound (2.11 g, 5.94 mmol, 92%). ^{1}H NMR (400 MHz, $CDCl_3$): δ 8.64 (s, 1H), 8.16 (s, 1H), 7.78 (dd, *J* = 8.1, 1.2 Hz, 1H), 7.32-7.27 (m, 1H), 7.24 – 7.16 (m, 2H), 6.59 (s, 1H), 1.53 (s, 9H). ^{13}C NMR (101 MHz, $CDCl_3$): δ 158.3, 157.4, 154.8, 154.7, 130.9, 130.2, 126.6, 126.5, 126.4, 124.9, 114.4, 82.0, 28.4.

Synthesis of N^1-(2,5-dichloropyrimidin-4-yl)benzene-1,2-diamine (11)

Compound **10** (323 mg, 0.91 mmol) was dissolved in DCM (10 mL), after which TFA (3 mL) was slowly added. The reaction mixture was stirred at rt for 16 h and subsequently evaporated to dryness. The residue was dissolved in water, neutralized with aqueous K_2CO_3 to pH 7-8 and the resulting precipitate was collected by filtration and dried to yield the title compound (197 mg, 0.77 mmol, 85%). ^{1}H NMR (400 MHz, DMSO): δ 9.01 (s, 1H), 8.14 (s, 1H), 7.03 (d, *J* = 7.8 Hz, 1H), 6.95 (s, 1H), 6.72 (d, *J* = 8.0 Hz, 1H), 6.54 (t, *J* = 7.5 Hz, 1H), 4.92 (s, 2H). ^{13}C NMR (101 MHz, DMSO): δ 158.7, 158.2, 157.3, 154.4, 144.9, 128.4, 127.8, 121.7, 115.8, 115.6.

Synthesis of N-(2-((2,5-dichloropyrimidin-4-yl)amino)phenyl)acrylamide (12)

Compound **11** (250 mg, 0.98 mmol) was dissolved in DCM (5 mL) and cooled to 0 °C. Subsequently, DIPEA (127 mg, 0.98 mmol) was added and the reaction mixture was stirred for 10 min. Acryloyl chloride (93 mg, 1.03 mmol) dissolved in DCM (1 mL) was dropwisely added to the mixture. After stirring for 1 h, the reaction was quenched by addition of water (50 mL). The mixture was extracted with DCM (50 mL), the organic extract was dried over $MgSO_4$ and concentrated. The crude residue was purified by flash column chromatography (20% → 40% EtOAc in pentane) to yield the title compound (259 mg, 0.84 mmol, 85%). ^{1}H NMR (400 MHz, $CDCl_3$): δ 8.72 (d, *J* = 18.0 Hz, 2H), 8.13 (s, 1H), 7.72 (dd, *J* = 8.2, 1.3 Hz, 1H), 7.26 (td, *J* = 7.8, 1.5 Hz, 1H), 7.08 (td, *J* = 7.7, 1.4 Hz, 1H), 6.95 (dd, *J* = 8.0, 1.5 Hz, 1H), 6.44 (dd, *J* = 16.9, 1.4 Hz, 1H), 6.30 (dd, *J* = 16.9, 10.1 Hz, 1H), 5.77 (dd, *J* = 10.1, 1.6 Hz, 1H). ^{13}C NMR (101 MHz, $CDCl_3$): δ 165.2, 157.8, 157.2, 154.7, 131.1, 129.8, 129.8, 129.0, 127.0, 126.3, 125.8, 125.0, 114.6.

Synthesis of 3-methoxy-4-nitrophenol (13)

3-Fluoro-4-nitrophenol (1.00 g, 6.4 mmol) was added to a solution of NaOMe in MeOH (0.5M, 14 mL), which was then heated at 50 °C for 12 h. Additional NaOMe in MeOH (0.5M, 14 mL) was added and the mixture was stirred at 50 °C until TLC indicated complete depletion of starting material. The mixture was diluted with H_2O (100 mL), neutralized with 3M HCl and the product was extracted with EtOAc (3 x 100 mL). The combined organic layers were washed with brine (100 mL), dried over $MgSO_4$ and evaporated to yield the title compound (1.01 g, 6.0 mmol, 94%). ^{1}H NMR (400 MHz, DMSO): δ 10.90 (s, 1H), 7.89 (d, *J* = 9.0 Hz, 1H), 6.60 (d, *J* = 2.4 Hz, 1H), 6.47 (dd, *J* = 9.0, 2.4 Hz, 1H), 3.86 (s, 3H). ^{13}C NMR (101 MHz, DMSO): δ 164.4, 156.1, 131.2, 128.8, 108.0, 100.8, 56.8. Spectroscopic data are in accordance with those reported in literature.[54]

Synthesis of 2-methoxy-1-nitro-4-(prop-2-yn-1-yloxy)benzene (14)

Compound **13** (600 mg, 3.6 mmol) and K_2CO_3 (1.47 g, 10.6 mmol) were taken up in DMF (10 mL) and heated at 60 °C for 30 min. The reaction mixture was cooled to rt, after which propargyl bromide (1.34 g, 9.0 mmol as 80% (w/w) solution in toluene) was added. The mixture was stirred at rt for 16 h, after which it was poured into ice water (200 mL) with stirring for 10 min. The formed precipitate was collected by filtration and dried under vacuum to yield the title compound (648 mg, 3.1 mmol, 88%), which was directly used in the next reaction.

Synthesis of 2-methoxy-4-(prop-2-yn-1-yloxy)aniline (15)

Compound **14** (600 mg, 2.9 mmol) was dissolved in 1,4-dioxane (10 mL) and cooled to 0 °C. Cooled (0 °C) stannous chloride dihydrate (3.28 g, 14.5 mmol) in concentrated HCl (10 mL) was dropwisely added to the reaction mixture. After stirring for 16 h at rt, the mixture was basified to pH >9 by addition of NaOH pellets and extracted with DCM (4 x 10 mL). The organic layer was washed with brine (10 mL), dried over $MgSO_4$ and concentrated to dryness. The crude product was then purified by flash column chromatography (0% → 25% EtOAc in pentane) to yield the title compound (395 mg, 2.23 mmol, 77%). ^{1}H NMR (400 MHz, $CDCl_3$): δ 6.62 (d, *J* = 8.4 Hz, 1H), 6.52 (d, *J* = 2.6 Hz, 1H), 6.42 (dd, *J* = 8.5, 2.6 Hz, 1H), 4.61 (d, *J* = 2.4 Hz, 2H), 3.81 (s, 3H), 3.49 (s, 2H), 2.51 (t, *J* = 2.4 Hz, 1H). ^{13}C NMR (101 MHz, $CDCl_3$): δ 151.0, 148.3, 130.8, 115.0, 105.9, 100.7, 79.3, 75.3, 56.8, 55.6.

Synthesis of N-(2-((5-chloro-2-((2-methoxy-4-(prop-2-yn-1-yloxy)phenyl)amino)pyrimidin-4-yl)amino)-phenyl)acrylamide (6, WEL028)

Compound **12** (46 mg, 0.15 mmol) and compound **15** (26 mg, 0.15 mmol) were taken up in isopropanol (5 mL), followed by the addition of *p*-TSA (28 mg, 0.15 mmol). The reaction mixture was heated under reflux for 16 h, after which it was concentrated under reduced pressure. The residue was taken up in saturated aqueous $NaHCO_3$ (20 mL) and the product was extracted with EtOAc (20 mL). The organic layer was dried over $MgSO_4$ and concentrated to dryness. The crude residue was purified by flash column chromatography (10% → 35% EtOAc in pentane) to yield the title compound (24 mg, 0.05 mmol, 36%). HRMS (ESI+) m/z: calculated for $C_{23}H_{20}ClN_5O_3$ ([M+H]): 450.13274; found: 450.13231.

^{1}H NMR (400 MHz, $CDCl_3$): δ 8.04 (d, *J* = 17.6 Hz, 2H), 7.87 (d, *J* = 8.9 Hz, 1H), 7.67 (s, 1H), 7.59 (t, *J* = 4.8 Hz, 2H), 7.38 (s, 1H), 7.29 (dd, *J* = 6.0, 3.5 Hz, 2H), 6.52 (d, *J* = 2.7 Hz, 1H), 6.40 – 6.31 (m, 2H), 6.16 (dd, *J* = 16.9, 10.3 Hz, 1H), 5.72 (d, *J* = 10.2 Hz, 1H), 4.65 (d, *J* = 2.4 Hz, 2H), 3.81 (s, 3H), 2.54 (t, *J* = 2.4 Hz, 1H). ^{13}C NMR (101 MHz, $CDCl_3$): δ 164.6, 157.8, 156.9, 153.5, 149.6, 131.6, 131.1, 130.8, 128.4, 127.2, 126.8, 126.4, 125.1, 123.2, 120.1, 105.1, 99.8, 78.9, 75.7, 56.5, 55.9.

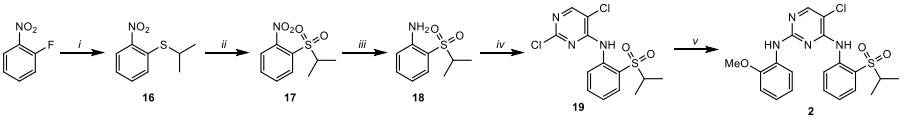

Supplementary Scheme 2.1 – Synthesis of compound 2. Reagents and conditions: *i*) 2-propanethiol, K_2CO_3, DMF, 100 °C, 98%. *ii*) *m*-CPBA, DCM, rt, 98%. *iii*) Pd/C, H_2, MeOH, rt, quant. *iv*) 2,4,5-trichloropyrimidine, NaH, DMF/DMSO (9:1), 0 °C to rt, 37%. *v*) *o*-anisidine, Xantphos, $Pd(OAc)_2$, Cs_2CO_3, 1,4-dioxane, 100 °C, 15%.

Synthesis of isopropyl(2-nitrophenyl)-sulfane (16)

1-Fluoro-2-nitrobenzene (9.88 g, 70 mmol) was dissolved in DMF (100 mL), followed by the addition of 2-propanethiol (5.47 g, 70 mmol) and K_2CO_3 (24.19 g, 175 mmol). The reaction mixture was heated at 100 °C for 16 h and subsequently cooled to rt. The mixture was diluted with H_2O (200 mL) and the product was extracted with EtOAc (3 x 200 mL). The organic layers were combined, dried over Na_2SO_4 and concentrated to yield the title compound (13.5 g, 68 mmol, 98%). ^{1}H NMR (400 MHz, $CDCl_3$): δ 8.12 (dd, *J* = 8.3, 1.5 Hz, 1H), 7.54 (ddd, *J* = 8.4, 7.1, 1.4 Hz, 1H), 7.48 (dd, *J* = 8.1, 1.4 Hz, 1H), 7.25 (ddd, *J* = 8.4, 7.1, 1.5 Hz, 1H), 3.58 (p, *J* = 6.6 Hz, 1H), 1.40 (d, *J* = 6.6 Hz, 6H). ^{13}C NMR (101 MHz, $CDCl_3$): δ 147.2, 136.5, 133.3, 128.3, 125.9, 124.9, 35.8, 22.4.

Synthesis of 1-(isopropylsulfonyl)-2-nitrobenzene (17)

Compound **16** (12.2 g, 61.3 mmol) was dissolved in DCM (120 mL), followed by portion wise addition of 3-chloroperbenzoic acid (31.6 g, 143 mmol) The reaction mixture was stirred at rt for 16 h. The mixture was diluted with 10% Na_2SO_3 (120 mL) and stirred for 10 min, after which layers were separated and the aqueous layer was extracted with DCM (3 x 120 mL). The organic layers were combined, washed with sat. $NaHCO_3$ (2 x 200 mL), brine (1 x 250 mL), dried over $MgSO_4$ and concentrated to yield the title compound (13.9 g, 60.7 mmol, 98%). ^{1}H NMR (400 MHz, $CDCl_3$): δ 8.15 – 8.07 (m, 1H), 7.86 – 7.72 (m, 3H), 4.04-3.95 (m, 1H), 1.41 (d, *J* = 6.8 Hz, 6H). ^{13}C NMR (101 MHz, $CDCl_3$): δ 134.8, 133.1, 132.2, 125.1, 56.0, 15.5.

Synthesis of 2-(isopropylsulfonyl)aniline (18)

Compound **17** (2.03 g, 8.85 mmol) was dissolved in MeOH (25 mL), followed by addition of Pd/C (93 mg, 0.87 mmol). The mixture was stirred under H_2 atmosphere for 16 h at rt, after which it was filtered over celite and concentrated to yield the title compound (1.76 g, 8.85 mmol, quant.). ^{1}H NMR (400 MHz, $CDCl_3$): δ 7.64 (dd, *J* = 8.0, 1.5 Hz, 1H), 7.40 – 7.30 (m, 1H), 6.80 (m, 1H), 6.74 (d, *J* = 8.2 Hz, 1H), 4.49 (s, 2H), 3.34 (m, 1H), 1.31 (d, *J* = 6.7 Hz, 6H). ^{13}C NMR (101 MHz, $CDCl_3$): δ 147.2, 135.2, 131.4, 118.3, 117.7, 117.7, 54.3, 15.4.

Synthesis of 2,5-dichloro-N-(2-(isopropylsulfonyl)phenyl)pyrimidin-4-amine (19)

A mixture of DMF/DMSO (9:1 ratio, 10 mL) was cooled to 0 °C, after which NaH (354 mg, 14.8 mmol) was added. Compound **18** (1.15 g, 5.77 mmol) was dissolved in DMF/DMSO (5 mL) and added to the reaction mixture. The suspension was stirred at 0 °C for 30 min, followed by the addition of 2,4,5-trichloropyrimidine (1.94 g, 10.6 mmol) diluted in DMF/DMSO (5 mL). The mixture was allowed to warm to rt and was then stirred for 16 h. The reaction mixture was diluted with H_2O (150 mL) and extracted with EtOAc (50 mL). The organic layer was washed with H_2O (5 x 50 mL), 5% LiCl (50 mL) and brine (50 mL), dried over $MgSO_4$ and subsequently concentrated. The crude residue was purified by flash column chromatography (0% → 20% EtOAc in pentane) to yield the title compound (777 mg, 2.24 mmol, 37%). ^{1}H NMR (400 MHz, $CDCl_3$): δ 10.06 (s, 1H), 8.62 (dd, *J* = 8.5, 1.2 Hz, 1H), 8.30 (s, 1H),

7.92 (dd, *J* = 8.0, 1.7 Hz, 1H), 7.75-7.71 (m, 1H), 7.37-7.27 (m, 1H), 3.26-3.16 (m, 1H), 1.31 (d, *J* = 6.8 Hz, 6H). ^{13}C NMR (101 MHz, $CDCl_3$): δ 157.9, 156.4, 155.7, 137.5, 135.3, 131.6, 124.7, 124.3, 122.8, 115.4, 56.2, 15.5.

Synthesis of 5-chloro-N^4-(2-(isopropylsulfonyl)phenyl)-N^2-(2-methoxyphenyl)pyrimidine-2,4-diamine (2)

Compound **19** (399 mg, 1.15 mmol), *o*-anisidine (142 mg, 1.15 mmol), XantPhos (67 mg, 0.12 mmol), $Pd(OAc)_2$ (14 mg, 0.06 mmol) and Cs_2CO_3 (756 mg, 2.30 mmol) were dissolved in 1,4-dioxane (15 mL) and the resulting mixture was heated at 100 °C for 16 h. The reaction mixture was diluted with EtOAc (50 mL), filtered over celite and subsequently concentrated. The crude residue was purified by flash column chromatography (0% → 30% EtOAc in pentane) to yield the title compound (77 mg, 0.18 mmol, 15%). HRMS (ESI+) m/z: calculated for $C_{20}H_{21}ClN_4O_3S$ ([M+H]): 433.10957; found: 433.10837. ^{1}H NMR (400 MHz, DMSO): δ 9.53 (s, 1H), 8.53 (d, *J* = 8.4 Hz, 1H), 8.37 (s, 1H), 8.25 (s, 1H), 7.82 (dd, *J* = 8.0, 1.6 Hz, 1H), 7.72 (dd, *J* = 7.9, 1.5 Hz, 1H), 7.66-7.62 (m, 1H), 7.38-7.29 (m, 1H), 7.14-7.02 (m, 2H), 6.92-6.88 (m, 1H), 3.79 (s, 3H), 3.47-3.40 (m, 1H), 1.15 (d, *J* = 6.8 Hz, 6H). ^{13}C NMR (101 MHz, DMSO): δ 158.6, 155.8, 155.3, 151.3, 138.5, 135.3, 131.4, 128.5, 124.6, 124.5, 124.0, 123.9, 123.5, 120.6, 111.6, 105.1, 56.0, 55.3, 15.3.

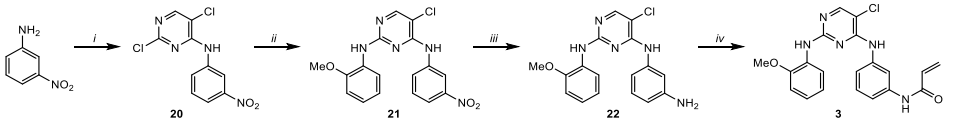

Supplementary Scheme 2.2 – Synthesis of compound 3. Reagents and conditions: *i*) 2,4,5-trichloropyrimidine, DIPEA, DMF, 70 °C, 99%. *ii*) *o*-anisidine, *p*-TSA, isopropanol, reflux, 36%. *iii*) PtO_2, H_2, THF, rt, 97%. *iv*) acryloyl chloride, DIPEA, DCM, 0 °C, 68%.

Synthesis of 2,5-dichloro-N-(3-nitrophenyl)pyrimidin-4-amine (20)

2,4,5-Trichloropyrimidine (1.42 g, 7.74 mmol) and DIPEA (2.00 g, 15.5 mmol) were dissolved in DMF (4 mL). To the stirring solution was added 3-nitroaniline (1.07 g, 7.74 mmol), after which the reaction mixture was heated at 70 °C for 16 h. The mixture was allowed to cool down to rt and subsequently diluted with EtOAc (75 mL) and washed with H_2O (3 x 50 mL). The organic layer was dried over $MgSO_4$ and concentrated to dryness to yield the title compound (2.18 g, 7.66 mmol, 99%). ^{1}H NMR (400 MHz, DMSO): δ 9.96 (s, 1H), 8.63 (t, *J* = 2.2 Hz, 1H), 8.49 (s, 1H), 8.17 – 8.09 (m, 1H), 8.01 (ddd, *J* = 8.3, 2.3, 0.9 Hz, 1H), 7.68 (t, *J* = 8.2 Hz, 1H). ^{13}C NMR (101 MHz, DMSO): δ 157.0, 156.2, 147. 8, 139.0, 129.9, 129.0, 122.5, 119.1, 117.2, 114.2.

Synthesis of 5-chloro-N^2-(2-methoxyphenyl)-N^4-(3-nitrophenyl)pyrimidine-2,4-diamine (21)

Compound **20** (600 mg, 2.10 mmol) and *o*-anisidine (259 mg, 2.10 mmol) were taken up in isopropanol (20 mL), followed by the addition of *p*-TSA (400 mg, 2.10 mmol). The reaction mixture was heated under reflux for 16 h, after which it was concentrated under reduced pressure. The residue was taken up in saturated aqueous $NaHCO_3$ (20 mL) and the product was extracted with EtOAc (20 mL). The organic layer was concentrated under reduced pressure and the crude residue was purified by flash column chromatography (10% → 30% EtOAc in pentane) to yield the title compound (284 mg, 0.38 mmol, 36%). ^{1}H NMR (400 MHz, DMSO): δ 9.31 (s, 1H), 8.51 (t, *J* = 2.2 Hz, 1H), 8.23 – 8.15 (m, 2H), 8.09 (s, 1H), 7.92 (ddd, *J* = 8.2, 2.3, 0.9 Hz, 1H), 7.81 – 7.74 (m, 1H), 7.55 (t, *J* = 8.2 Hz, 1H), 7.04 – 6.98 (m, 2H), 6.80 – 6.74 (m, 1H), 3.80 (s, 3H). ^{13}C NMR (101 MHz, DMSO): δ 157.8, 155.6, 155.5, 150.0, 147.7, 140.0, 129.5, 128.5, 128.1, 123.5, 121.8, 120.0, 117.8, 116.8, 110.9, 104.3, 55.6.

Synthesis of N^4-(3-aminophenyl)-5-chloro-N^2-(2-methoxyphenyl)pyrimidine-2,4-diamine (22)

Compound **21** (200 mg, 0.54 mmol) was dissolved in THF (10 mL), followed by addition of PtO_2 (21 mg, 0.09 mmol). The mixture was stirred under H_2 atmosphere at rt for 72 h, after which it was diluted

in MeOH, filtered over celite and concentrated to yield the title compound (179 mg, 0.54 mmol, 97%), which was directly used in the next step.

Synthesis of N-(3-((5-chloro-2-((2-methoxyphenyl)amino)pyrimidin-4-yl)amino)phenyl)acrylamide (3)

Compound **22** (77 mg, 0.23 mmol) was taken up in DCM (2 mL) and cooled to 0 °C. Subsequently, DIPEA (29 mg, 0.23 mmol) was added and the reaction mixture was stirred for 10 min. Acryloyl chloride (20 mg, 0.23 mmol) dissolved in DCM (1 mL) was dropwisely added to the mixture. After stirring for 30 min, the reaction was quenched by addition of water (5 mL). The product was extracted from the reaction mixture with DCM (3 x 25 mL) and the organic layer was dried over $MgSO_4$ and concentrated to dryness. The crude residue was purified by flash column chromatography (10% → 40% EtOAc in pentane) to yield the title compound (61 mg, 0.15 mmol, 68%). HRMS (ESI+) m/z: calculated for $C_{20}H_{18}ClN_5O_2$ ([M+H]): 396.12218; found: 396.12156. ^{1}H NMR (400 MHz, $CDCl_3$): δ 8.21 (dd, *J* = 7.9, 1.6 Hz, 1H), 8.04 (d, *J* = 12.2 Hz, 2H), 7.70 (s, 1H), 7.58 (d, *J* = 7.9 Hz, 1H), 7.41 (s, 1H), 7.33 (t, *J* = 8.0 Hz, 1H), 7.26 (d, *J* = 8.5 Hz, 1H), 7.16 (s, 1H), 7.04 – 6.95 (m, 1H), 6.94 – 6.83 (m, 2H), 6.45 (dd, *J* = 16.9, 1.3 Hz, 1H), 6.23 (dd, *J* = 16.8, 10.2 Hz, 1H), 5.79 (dd, *J* = 10.2, 1.3 Hz, 1H), 3.88 (s, 3H). ^{13}C NMR (101 MHz, $CDCl_3$): δ 155.7, 148.8, 138.6, 138.5, 131.2, 129.6, 128.8, 128.2, 122.6, 120.5, 120.1, 117.3, 116.5, 115.7, 112.8, 110.3, 105.1, 55.8.

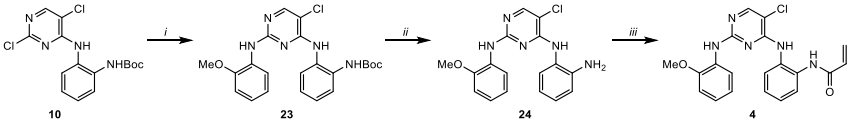

Supplementary Scheme 2.3 – Synthesis of compound 4. Reagents and conditions: *i*) *o*-anisidine, Xantphos, $Pd(OAc)_2$, Cs_2CO_3, 1,4-dioxane, 100 °C, 6%. *ii*) TFA, DCM, rt. *iii*) acryloyl chloride, DIPEA, DCM, 0 °C, 45% over 2 steps.

Synthesis of tert-butyl(2-((5-chloro-2-((2-methoxyphenyl)amino)pyrimidin-4-yl)amino)phenyl)carbamate (23)

Compound **10** (600 mg, 1.69 mmol), *o*-anisidine (208 mg, 1.69 mmol), Xantphos (98 mg, 0.17 mmol), $Pd(OAc)_2$ (19 mg, 0.084 mmol) and cesium carbonate (1.10 g, 3.38 mmol) were dissolved in 20 mL 1,4-dioxane. The reaction mixture was purged with argon and subsequently heated at 100 °C for 16 h. Subsequently, the mixture was diluted with EtOAc and filtered over Celite®, after which the filtrate was concentrated. The crude residue was purified by flash column chromatography (0% → 20% EtOAc in pentane) to yield the title compound (48 mg, 0.11 mmol, 6%). ^{1}H NMR (400 MHz, $CDCl_3$): δ 8.12 – 8.03 (m, 2H), 7.79 (s, 1H), 7.72 – 7.66 (m, 1H), 7.63 (s, 1H), 7.49 – 7.41 (m, 1H), 7.29 – 7.22 (m, 2H), 6.89 (m, 1H), 6.82 (dd, *J* = 8.1, 1.5 Hz, 1H), 6.78 – 6.70 (m, 1H), 6.66 (s, 1H), 3.85 (s, 3H), 1.50 (s, 9H). ^{13}C NMR (101 MHz, $CDCl_3$): δ 157.0, 154.1, 147.8, 131.9, 130.9, 129.2, 128.9, 127.6, 126.5, 125.4, 123.9, 121.6, 120.8, 118.7, 114.2, 109.8, 105.2, 81.5, 55.8, 28.4.

Synthesis of N^4-(2-aminophenyl)-5-chloro-N^2-(2-methoxyphenyl)pyrimidine-2,4-diamine (24)

Compound **23** (50 mg, 0.11 mmol) was dissolved in DCM (3 mL), after which TFA (3 mL) was slowly added. The reaction mixture was stirred at rt for 16 h and subsequently evaporated to dryness to yield the title compound, which was directly used in the next reaction.

Synthesis of N-(2-((5-chloro-2-((2-methoxyphenyl)amino)pyrimidin-4-yl)amino)phenyl)acrylamide (4)

Compound **24** (84 mg, 0.18 mmol) was taken up in DCM (2 mL) and cooled to 0 °C. Subsequently, DIPEA (24 mg, 0.18 mmol) was added and the reaction mixture was stirred for 10 min. Acryloyl chloride (17 mg, 0.18 mmol) dissolved in DCM (1 mL) was dropwisely added to the mixture. After stirring for 15 min, the reaction was quenched by addition of water (5 mL). The product was extracted from the reaction mixture with DCM (50 mL) and the organic layer was dried over $MgSO_4$ and concentrated to

dryness. The crude residue was purified by flash column chromatography (10% → 40% EtOAc in pentane) to yield the title compound (20 mg, 0.05 mmol, 45% over two steps). HRMS (ESI+) m/z: calculated for $C_{20}H_{18}ClN_5O_2$ ([M+H]): 396.12218; found: 396.12156. ^{1}H NMR (400 MHz, MeOD): δ 8.04 (s, 1H), 7.81 (dd, *J* = 8.1, 1.6 Hz, 1H), 7.76 – 7.69 (m, 1H), 7.51 – 7.44 (m, 1H), 7.41 – 7.33 (m, 2H), 7.03 – 6.95 (m, 2H), 6.73 (ddd, *J* = 8.6, 7.1, 1.8 Hz, 1H), 6.48 (dd, *J* = 17.0, 9.5 Hz, 1H), 6.40 (dd, *J* = 16.9, 2.4 Hz, 1H), 5.81 (dd, *J* = 9.4, 2.4 Hz, 1H), 3.87 (s, 3H). ^{13}C NMR (101 MHz, MeOD): δ 166.9, 158.8, 149.9, 132.9, 132.5, 131.4, 129.9, 129.2, 128.9, 128.2, 127.9, 127.4, 126.0, 125.5, 125.0, 122.0, 121.6, 111.5, 106.5, 56.3.

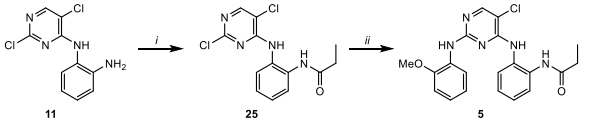

Supplementary Scheme 2.4 – Synthesis of compound 5. Reagents and conditions: *i*) propionyl chloride, DIPEA, DCM, 0 °C, 52%. *ii*) *o*-anisidine, *p*-TSA, isopropanol, reflux, 56%.

Synthesis of N-(2-((2,5-dichloropyrimidin-4-yl)amino)phenyl)propionamide (25)

Compound **11** (171 mg, 0.67 mmol) was dissolved in DCM (5 mL) and cooled to 0 °C. Subsequently, DIPEA (85 mg, 0.67 mmol) was added and the reaction mixture was stirred for 10 min. Propionyl chloride (64 mg, 0.67 mmol) dissolved in DCM (3 mL) was dropwisely added. After stirring for 2 h, the reaction mixture was diluted with DCM (50 mL) and washed with H_2O (2 x 50 mL). The organic extract was dried over $MgSO_4$ and concentrated to dryness. The crude residue was purified by flash column chromatography (20% → 30% EtOAc in pentane) to yield the title compound (109 mg, 0.35 mmol, 52%). ^{1}H NMR (400 MHz, $CDCl_3$): δ 8.67 (s, 1H), 8.16 (s, 1H), 8.07 (s, 1H), 7.73 (dd, *J* = 8.2, 1.3 Hz, 1H), 7.32 – 7.23 (m, 1H), 7.14 – 7.05 (m, 1H), 6.87 (dd, *J* = 7.9, 1.5 Hz, 1H), 2.38 (q, *J* = 7.6 Hz, 2H), 1.20 (t, *J* = 7.6 Hz, 3H). ^{13}C NMR (101 MHz, $CDCl_3$): δ 174.4, 158.1, 157.4, 155.0, 131.4, 130.2, 127.0, 126.5, 126.1, 125.0, 114.7, 30.0, 10.2.

Synthesis of N-(2-((5-chloro-2-((2-methoxyphenyl)amino)pyrimidin-4-yl)amino)phenyl)propionamide (5)

Compound **25** (59 mg, 0.19 mmol) and *o*-anisidine (23 mg, 0.19 mmol) were taken up in isopropanol (10 mL), followed by the addition of *p*-TSA (37 mg, 0.19 mmol). The reaction mixture was heated under reflux for 16 h, after which it was concentrated under reduced pressure. The residue was taken up in saturated aqueous $NaHCO_3$ (20 mL) and the product was extracted with EtOAc (20 mL). The organic layer was dried over $MgSO_4$ and concentrated. The crude residue was purified by flash column chromatography (10% → 40% EtOAc in pentane), affording a mixture of compound **25** and **5** that was further purified by HPLC to yield the title compound (42 mg, 0.10 mmol, 56%). HRMS (ESI+) m/z: calculated for $C_{20}H_{20}ClN_5O_2$ ([M+H]): 398.13783; found: 398.13722. ^{1}H NMR (400 MHz, $CDCl_3$): δ 10.04 (s, 1H), 9.24 (s, 1H), 7.85 (s, 1H), 7.68 – 7.60 (m, 2H), 7.58 (dd, *J* = 8.0, 1.6 Hz, 1H), 7.26 (s, 3H), 7.16 (dd, *J* = 7.5, 2.0 Hz, 1H), 7.06 (ddd, *J* = 8.3, 7.6, 1.6 Hz, 1H), 6.84 (dd, *J* = 8.3, 1.4 Hz, 1H), 6.70 (td, *J* = 7.8, 1.3 Hz, 1H), 3.80 (s, 3H), 2.46 (q, *J* = 7.5 Hz, 2H), 1.26 (t, *J* = 7.6 Hz, 3H). ^{13}C NMR (101 MHz, $CDCl_3$): δ 174.3, 157.7, 153.3, 152.8, 151.2, 130.6, 127.8, 127.6, 126.9, 126.1, 125.8, 124.9, 123.1, 120.3, 111.0, 105.4, 56.0, 30.3, 10.2.

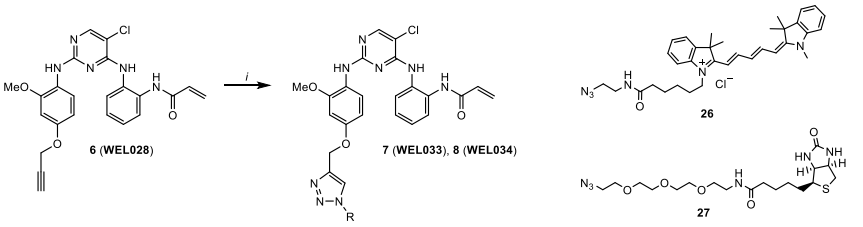

Supplementary Scheme 2.5 – Synthesis of one-step probes 7 and 8. *i*) 26 or 27, $CuSO_4$, sodium ascorbate, H_2O/DCM (1:1), rt, 5% (7) or 17% (8) after HPLC purification.

Synthesis of 1-(6-((2-(4-((4-((4-((2-acrylamidophenyl)amino)-5-chloropyrimidin-2-yl)amino)-3-methoxy-phenoxy)methyl)-1H-1,2,3-triazol-1-yl)ethyl)amino)-6-oxohexyl)-3,3-dimethyl-2-((1E,3E)-5-((E)-1,3,3-trimethylindolin-2-ylidene)penta-1,3-dien-1-yl)-3H-indol-1-ium (7, WEL033)

Compound **6** (30 mg, 0.07 mmol) and Cy5-azide **26** (77 mg, 0.14 mmol) were dissolved in degassed DCM (3 mL). $CuSO_4$ (8 mg, 0.01 mmol) and sodium ascorbate (16 mg, 0.03 mmol) were separately dissolved in degassed H_2O (3 mL) and added to the reaction mixture. The reaction mixture was vigorously stirred for 16 h at rt and subsequently evaporated to dryness. The crude residue was purified by flash column chromatography (DCM → 2% MeOH in DCM), followed by further HPLC purification to yield the title compound (3.2 mg, 3 µmol, 5%). HRMS (ESI+) m/z: calculated for $[C_{57}H_{63}ClN_{11}O_4]^+$: 1000.47475; found: 1000.47462. ^{1}H NMR (600 MHz, MeOD): δ 8.20 (td, *J* = 13.1, 3.2 Hz, 2H), 8.07 (s, 1H), 7.97 (s, 1H), 7.66 (dd, *J* = 7.8, 1.7 Hz, 1H), 7.52 – 7.45 (m, 4H), 7.39 (m, 2H), 7.35 – 7.30 (m, 2H), 7.29 (d, *J* = 7.1 Hz, 1H), 7.27 – 7.22 (m, 4H), 6.66 (d, *J* = 2.6 Hz, 1H), 6.57 (t, *J* = 12.4 Hz, 1H), 6.51 – 6.42 (m, 2H), 6.40 (dd, *J* = 16.9, 1.9 Hz, 1H), 6.27 (d, *J* = 13.7 Hz, 1H), 6.19 (d, *J* = 13.7 Hz, 1H), 5.82 (dd, *J* = 9.9, 1.9 Hz, 1H), 5.17 (s, 2H), 4.57 – 4.53 (m, 2H), 4.04 (t, *J* = 7.7 Hz, 2H), 3.77 (s, 3H), 3.69 – 3.65 (m, 2H), 3.56 (s, 3H), 2.66 (s, 3H), 2.15 (t, *J* = 7.2 Hz, 2H), 1.79 – 1.58 (m, 18H), 1.40 – 1.31 (m, 2H). ^{13}C NMR (151 MHz, MeOD): δ 176.2, 175.3, 174.6, 166.9, 155.4, 145.1, 144.2, 143.5, 142.6, 142.5, 133.0, 131.4, 129.8, 129.7, 129.0, 128.7, 128.1, 127.4, 126.6, 126.2, 126.2, 126.0, 125.6, 123.4, 123.2, 112.0, 111.8, 106.8, 104.3, 104.2, 100.7, 62.8, 56.4, 49.8, 44.8, 40.3, 36.5, 28.1, 27.9, 27.9, 27.8, 27.1, 26.4.

Synthesis of N-(2-(2-(2-(2-(4-((4-((4-((2-acrylamidophenyl)amino)-5-chloropyrimidin-2-yl)amino)-3-methox-yphenoxy)methyl)-1H-1,2,3-triazol-1-yl)ethoxy)ethoxy)ethoxy)ethyl)-5-((3aS,4S,6aR)-2-oxohexahydro-1H-thieno[3,4-d]imidazol-4-yl)pentanamide (8, WEL034)

Compound **6** (8.7 mg, 0.02 mmol) and biotin-PEG_3-azide **27** (9.1 mg, 0.01 mmol) were dissolved in degassed DCM (2 mL). $CuSO_4$ (2.3 mg, 0.01 mmol) and sodium ascorbate (4.4 mg, 0.02 mmol) were separately dissolved in degassed H_2O (2 mL) and added to the reaction mixture. The reaction mixture was vigorously stirred for 16 h at rt and subsequently evaporated to dryness. The crude residue was purified by HPLC to yield the title compound (3.0 mg, 3 µmol, 17%). HRMS (ESI+) m/z: calculated for $C_{41}H_{52}ClN_{11}O_8S$ [M+H]: 894.34823; found: 894.34883. ^{1}H NMR (600 MHz, MeOD): δ 8.14 (s, 1H), 8.00 (d, *J* = 19.0 Hz, 1H), 7.69 (dd, *J* = 7.9, 1.6 Hz, 1H), 7.49 (dd, *J* = 7.9, 1.5 Hz, 1H), 7.43 (s, 1H), 7.38 (td, *J* = 7.7, 1.6 Hz, 1H), 7.34 (td, *J* = 7.6, 1.5 Hz, 1H), 6.73 (d, *J* = 2.5 Hz, 1H), 6.49 (dd, *J* = 17.0, 9.9 Hz, 2H), 6.42 (dd, *J* = 17.0, 2.0 Hz, 1H), 5.84 (dd, *J* = 9.9, 2.0 Hz, 1H), 5.18 (s, 2H), 4.62 (dd, *J* = 5.5, 4.4 Hz, 2H), 4.46 (ddd, *J* = 7.9, 5.0, 0.9 Hz, 1H), 4.26 (dd, *J* = 7.9, 4.5 Hz, 1H), 3.90 (dd, *J* = 5.6, 4.4 Hz, 2H), 3.84 (s, 3H), 3.64 – 3.54 (m, 10H), 3.48 (t, *J* = 5.5 Hz, 2H), 3.16 (ddd, *J* = 9.0, 5.8, 4.5 Hz, 1H), 2.93 – 2.86 (m, 1H), 2.72 – 2.63 (m, 2H), 2.20 – 2.12 (m, 2H), 2.04 (s, 1H), 1.76 – 1.49 (m, 5H), 1.43 – 1.34 (m, 2H). ^{13}C NMR (151 MHz, MeOD): δ 176.1, 167.0, 166.1, 159.3, 154.9, 144.7, 133.2, 131.6, 131.4, 129.1, 128.9, 128.5, 127.5, 126.3, 126.0, 107.0, 100.9, 71.5, 71.4, 71.4, 71.2, 70.6, 70.3, 63.3, 62.7, 61.6, 57.0, 56.5, 51.5, 49.8, 49.6, 41.0, 40.3, 36.7, 29.8, 29.5, 26.8.

Supplementary Data

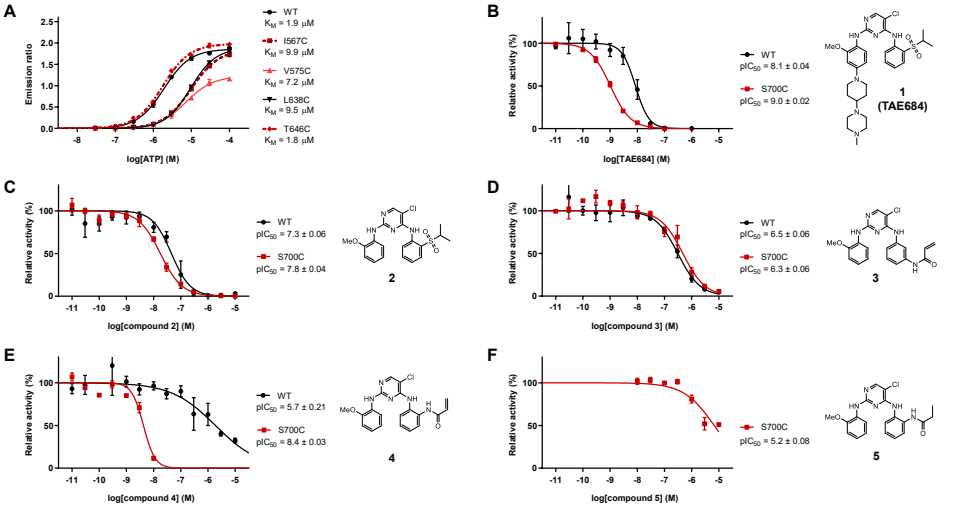

Supplementary Figure 2.1 - Determination of ATP K_M for other active FES mutants and concentration-response curves of inhibitors against FES^{WT} and FES^{S700C}. (A) Determination of ATP K_M for FES^{WT} and other FES mutants with >50% relative activity as determined in Figure 2.3B. **(B-F)** Concentration-response curves of inhibitors against FES^{WT} and FES^{S700C} as determined in TR-FRET assay. Compound code and structure is depicted right of the corresponding curve. Data represent means ± SEM (N = 3).

Supplementary Table 2.2 – Substrate identification using PamChip® activity assay. Top 30 of peptides with highest signal intensity are shown. Numbers behind substrate names indicate the amino acid residue numbers within the corresponding protein sequence. Predicted phosphorylated tyrosine residues are indicated in bold red.

Substrate	Peptide	log2 of signal intensity	
		FES^{WT}	FES^{S700C}
CD79A_181_193	EYEDENL**Y**EGLNL	14.59	14.18
ENOG_37_49	SGASTGI**Y**EALEL	14.39	14.13
ZAP70_313_325	SVYESP**Y**SDPEEL	12.83	12.51
EFS_246_258	GGTDEGI**Y**DVPLL	12.68	12.43
PLCG1_764_776	IGTAEPD**Y**GALYE	12.56	12.48
RET_1022_1034	TPSDSLI**Y**DDGLS	12.53	12.29
IRS2_626_638	HPYPED**Y**GDIEIG	12.38	12.20
EPHA1_774_786	LDDFDGT**Y**ETQGG	12.35	12.24
PGFRB_572_584	VSSDGHE**Y**IYVDP	12.33	12.09
P85A_600_612	NENTEDQ**Y**SLVED	12.27	12.19
LAT_249_261	EEGAPD**Y**ENLQEL	12.14	12.23
PLCG2_1191_1203_C1200S	ESEEEL**Y**SSSRQL	12.14	12.04
PDPK1_2_14	ARTTSQL**Y**DAVPI	12.10	11.97
FRK_380_392	KVDNEDI**Y**ESRHE	11.99	11.88
PTN11_57_67	QNTGD**Y**YDLYG	11.89	11.89
PTN11_580_590	SARV**Y**ENVGLM	11.71	11.71
KIT_930_942_C942S	ESTNHI**Y**SNLANS	11.68	11.59
PDPK1_369_381	DEDCYGN**Y**DNLLS	11.55	11.57
EGFR_1165_1177	ISLDNPD**Y**QQDFF	11.40	11.59
PECA1_708_718	DTETV**Y**SEVRK	11.36	11.53
PGFRB_709_721	RPPSAEL**Y**SNALP	11.35	11.53
EPHA7_607_619	TYIDPET**Y**EDPNR	11.30	11.43
VGFR2_989_1001	EEAPEDL**Y**KDFLT	11.26	11.38
PGFRB_1002_1014	LDTSSVL**Y**TAVQP	11.25	11.33
PTN6_558_570	KHKEDV**Y**ENLHTK	11.18	11.16
EPHA2_765_777	EDDPEAT**Y**TTSGG	11.16	11.32
PTN6_531_541	GQESE**Y**GNITY	11.15	11.29
FES_706_718	REEADGV**Y**AASGG	11.07	11.21
FER_707_719	RQEDGGV**Y**SSSGL	10.98	11.13
IRS1_890_902	PKSPGE**Y**VNIEFG	10.93	11.11

Supplementary Table 2.3 - SH2 binding partner identification using PamChip® binding assay. Top 30 of peptides with highest signal intensity are shown. Numbers behind substrate names indicate the amino acid residue numbers within the corresponding protein sequence.

Binding partner	Peptide	log2 of signal intensity	
		FES^{WT}	FES^{S700C}
PGFRB_572_584	VSSDGHEYIYVDP	12.44	13.06
PGFRB_1014_1028	PNEGDNDYIIPLPDP	12.17	12.94
LAT_249_261	EEGAPDYENLQEL	10.79	12.19
VGFR2_1168_1180	AQQDGKDYIVLPI	10.69	11.64
ENOG_37_49	SGASTGIYEALEL	10.67	12.29
PTN11_57_67	QNTGDYYDLYG	10.66	12.05
CD3E_182_194	PVPNPDYEPIRKG	10.03	11.48
CD79A_181_193	EYEDENLYEGLNL	10.02	12.05
IRS1_890_902	PKSPGEYVNIEFG	9.97	11.28
LAT_194_206	MESIDDYVNVPES	9.51	11.14
MAPK3_198_210_C203S	ALQTPSYTPYYVA	9.32	10.68
MK12_180_189_M182B	SEBTGYVVTR	9.16	10.58
PTN6_558_570	KHKEDVYENLHTK	8.74	10.88
FGFR2_762_774	TLTTNEEYLDLSQ	8.26	9.86
TYK2_1048_1060	VPEGHEYYRVRED	7.88	9.60
JAK3_974_986	LPLDKDYYVVREP	7.87	9.77
RON_1346_1358	SALLGDHYVQLPA	7.75	9.04
FGFR3_753_765	TVTSTDEYLDLSA	7.66	9.57
MET_1227_1239	RDMYDKEYYSVHN	7.59	9.42
PTN11_580_590	SARVYENVGLM	7.27	9.94
EGFR_1190_1202	STAENAEYLRVAP	7.12	9.01
MK14_173_185	RHTDDEMTGYVAT	7.08	9.11
FAK2_572_584	RYIEDEDYYKASV	7.00	9.11
JAK1_1027_1039	AIETDKEYYTVKD	6.53	8.78
MK03_199_208	GFLTEYVATR	6.49	8.31
EPOR_419_431	ASAASFEYTILDP	6.42	7.97
MK12_178_190	ADSEMTGYVVTRW	6.15	8.13
41_654_666	LDGENIYIRHSNL	6.08	8.02
MK07_212_224	AEHQYFMTEYVAT	4.96	6.25
HAVR2_257_267	GIRSEENIYTI	4.95	4.67

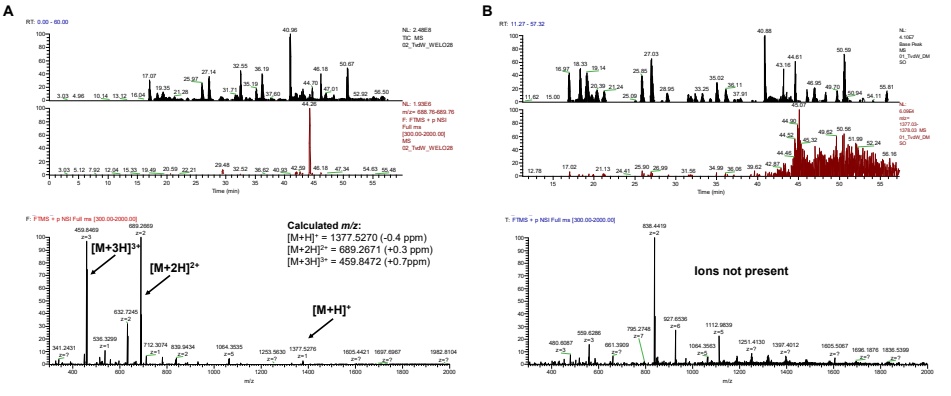

Supplementary Figure 2.2 - LC-MS elution profiles of FES^{S700C} incubated with WEL028 (A) or vehicle (B). Expected precursor ions and corresponding calculated m/z values are indicated. Ions were not present in vehicle-treated control sample.

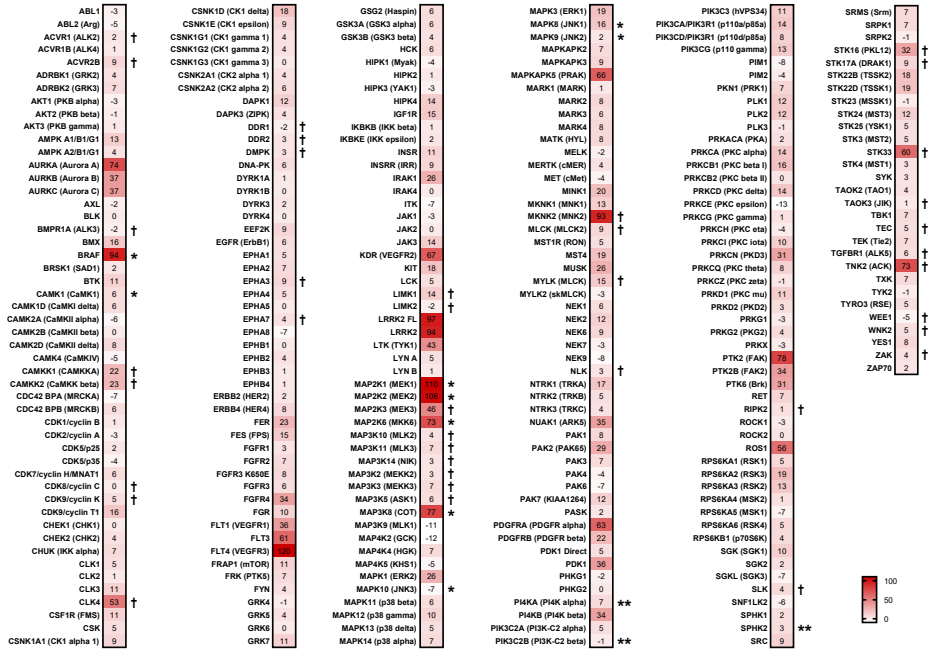

Supplementary Figure 2.3 - Single-point selectivity screen of WEL028 on a panel of 279 kinases. All data were obtained from SelectScreen™ selectivity profiling service. Assays were performed at 1 µM WEL028 with 1 h pre-incubation. The ATP concentration was equal to the kinase K_M, except for those indicated († = LanthaScreen technology, no ATP; * = 100 µM ATP; ** = 10 µM ATP). Values represent mean percentage inhibition compared to vehicle-treated control (N = 2).

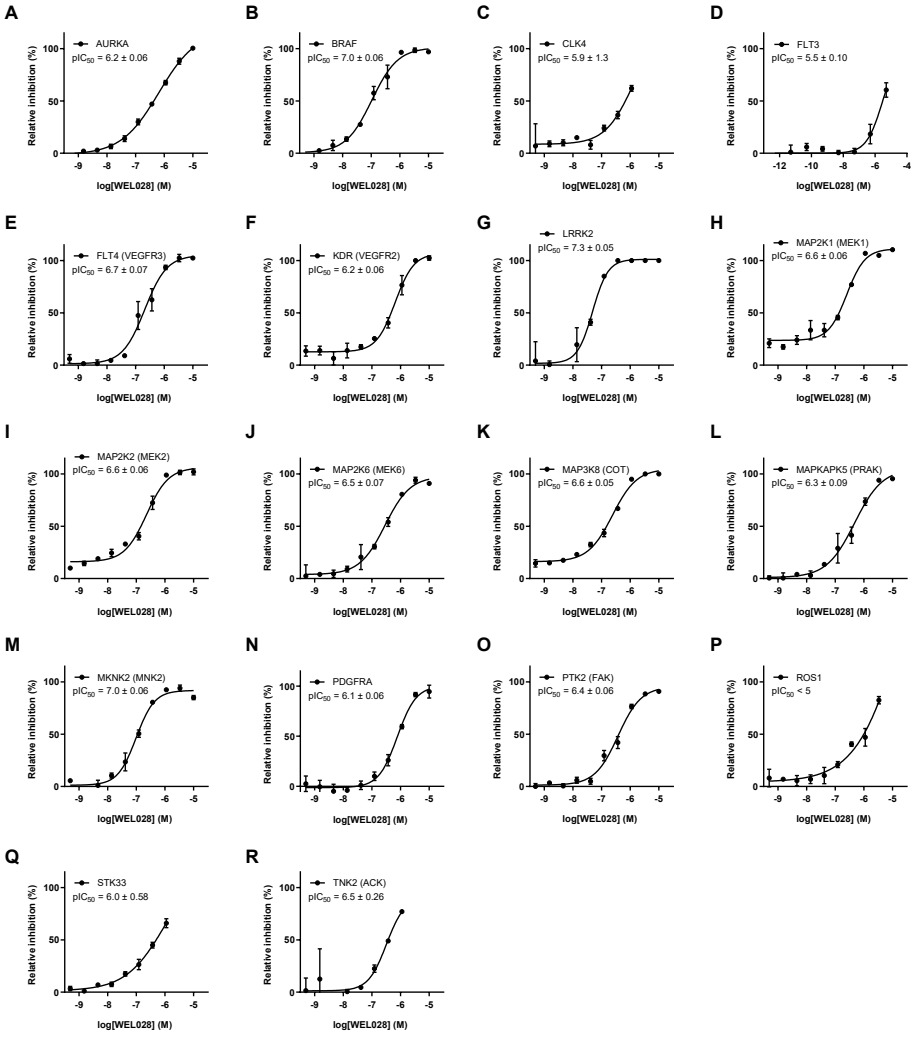

Supplementary Figure 2.4 - Concentration-response curves of WEL028 against kinases with >50% inhibition at 1 µM in initial single-dose screen. Data (means ± SD, N = 2) were obtained from SelectScreen™ selectivity profiling service. Assays were performed with 1 h pre-incubation and concentration of ATP was selected to be equal to the K_M, unless indicated otherwise in Supplementary Figure 2.3.

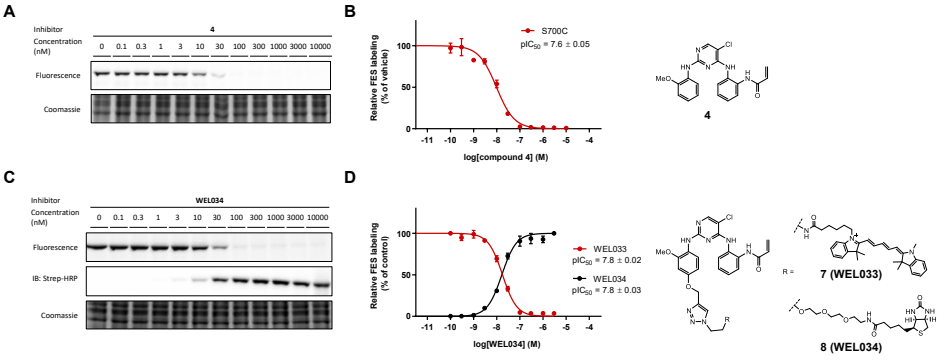

Supplementary Figure 2.5 - Competition of WEL033 labeling by compound 4 and biotin-conjugate 8 (WEL034). **(A, B)** Recombinantly expressed FES^{S700C} in HEK293T cell lysate was incubated with compound **4** (indicated concentrations, 30 min, rt), followed by two-step probe WEL028 (250 nM, 30 min, rt) and click mix containing Cy5-azide (2 eq., 30 min, rt). Samples were resolved by SDS-PAGE, followed by in-gel fluorescence scanning. Band intensities were normalized to vehicle-treated control. **(C, D)** Dose-dependent competition by WEL034. Samples were processed as described in A, but labeled with one-step probe WEL033 (250 nM, 30 min, rt). After in-gel fluorescence scanning, proteins were transferred to a PVDF membrane and immunoblotted against streptavidin-HRP. Band intensities (red: WEL033, black: WEL034) were normalized to vehicle-treated control (WEL033) or highest concentration (WEL034). Compound codes and structures are depicted right of the corresponding curves. Data represent means ± SEM (N = 3).

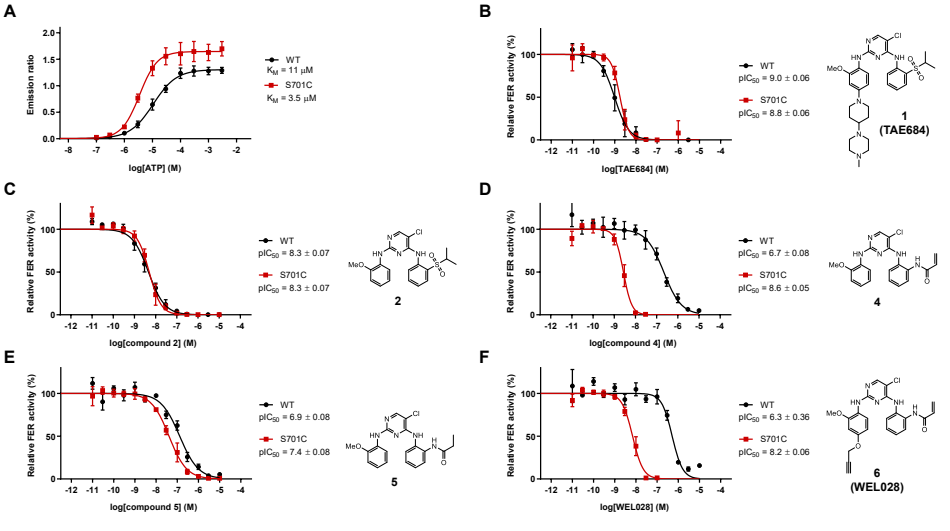

Supplementary Figure 2.6 - Determination of ATP K_M for FER^{WT} and FER^{S701C} and concentration-response curves of inhibitors against FER^{WT} and FER^{S701C}. **(A)** Determination of ATP K_M for FER^{WT} and FER^{S701C}. **(B-F)** Concentration-response curves of inhibitors against FER^{WT} and FER^{S701C} as determined in TR-FRET assay. Compound code and structure is depicted right of the corresponding curve. Data represent means ± SEM (N = 3).

Supplementary Table 2.4 - Inhibitory potency of synthesized TAE684 derivatives against FER^{WT} and FER^{S701C}. Half maximal inhibitory concentrations (expressed as pIC_{50}) were determined using recombinantly expressed FER^{WT} and FER^{S701C} in a TR-FRET assay. Final ATP concentration was 12 µM and 1 µM for FER^{WT} and FER^{S701C}, respectively. Apparent fold selectivity was calculated as IC_{50} on FER^{WT} divided by IC_{50} on FER^{S701C}. Data represent means ± SEM (N = 3). ND: not determined. Dose-response curves can be found in Supplementary Figure 2.6.

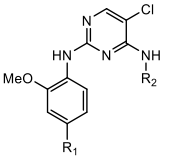

Compound	R_1	R_2	pIC_{50}		Apparent fold selectivity
			FER^{WT}	FER^{S701C}	
1 (**TAE684**)	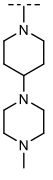	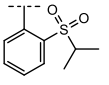	9.0 ± 0.06	8.8 ± 0.06	0.54
2	H	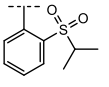	8.3 ± 0.07	8.3 ± 0.07	0.92
4	H	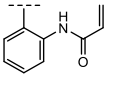	6.7 ± 0.08	8.6 ± 0.05	81
5	H	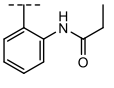	6.9 ± 0.08	7.4 ± 0.08	3.2
6 (**WEL028**)	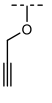	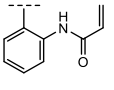	6.3 ± 0.06	8.2 ± 0.06	74

References

1. Ubersax, J. A. & Ferrell, J. E. Mechanisms of specificity in protein phosphorylation. *Nature Reviews Molecular Cell Biology* **8**, 530–541 (2007).
2. Manning, G., Whyte, D. B., Martinez, R., Hunter, T. & Sudarsanam, S. The protein kinase complement of the human genome. *Science* **298**, 1912–1934 (2002).
3. Zhang, J., Yang, P. & Gray, N. Targeting cancer with small molecule kinase inhibitors. *Nat. Rev. Cancer* **9**, 28–39 (2009).
4. Fedorov, O., Müller, S. & Knapp, S. The (un)targeted cancer kinome. *Nat. Chem. Biol.* **6**, 166–169 (2010).
5. Grimminger, F., Schermuly, R. T. & Ghofrani, H. A. Targeting non-malignant disorders with tyrosine kinase inhibitors. *Nature Reviews Drug Discovery* **9**, 956–970 (2010).
6. Roskoski, R. Properties of FDA-approved small molecule protein kinase inhibitors. *Pharmacological Research* **144**, 19–50 (2019).
7. Weir, M. C. *et al.* Dual inhibition of Fes and Flt3 tyrosine kinases potently inhibits Flt3-ITD+ AML cell growth. *PLoS One* **12**, e0181178 (2017).
8. Miyata, Y. *et al.* Pathological significance and predictive value for biochemical recurrence of c-Fes expression in prostate cancer. *Prostate* **72**, 201–208 (2012).
9. Asai, A. *et al.* Pathological significance and prognostic significance of FES expression in bladder cancer vary according to tumor grade. *J Cancer Res Clin Oncol* **1**, 1–11 (2017).
10. Haigh, J., McVeigh, J. & Greer, P. The fps/fes tyrosine kinase is expressed in myeloid, vascular endothelial, epithelial, and neuronal cells and is localized in the trans-golgi network. *Cell growth Differ.* **7**, 931–44 (1996).
11. Greer, P. Closing in on the biological functions of Fps/Fes and Fer. *Nat. Rev. Mol. Cell Biol.* **3**, 278–89 (2002).
12. Cheng, H. Y., Schiavone, A. P. & Smithgall, T. E. A Point Mutation in the N-Terminal Coiled-Coil Domain Releases c-Fes Tyrosine Kinase Activity and Survival Signaling in Myeloid Leukemia Cells. *Mol. Cell. Biol.* **21**, 6170–6180 (2001).
13. Di Fulvio, M. *et al.* Phospholipase D2 (PLD2) shortens the time required for myeloid leukemic cell differentiation: Mechanism of action. *J. Biol. Chem.* **287**, 393–407 (2012).
14. Filippakopoulos, P. *et al.* Structural Coupling of SH2-Kinase Domains Links Fes and Abl Substrate Recognition and Kinase Activation. *Cell* **134**, 793–803 (2008).
15. Takashima, Y., Delfino, F. J., Engen, J. R., Superti-Furga, G. & Smithgall, T. E. Regulation of c-Fes tyrosine kinase activity by coiled-coil and SH2 domains: Analysis with Saccharomyces cerevisiae. *Biochemistry* **42**, 3567–3574 (2003).
16. Rogers, J. A., Read, R. D., Li, J., Peters, K. L. & Smithgall, T. E. Autophosphorylation of the Fes tyrosine kinase. Evidence for an intermolecular mechanism involving two kinase domain tyrosine residues. *J. Biol. Chem.* **271**, 17519–17525 (1996).
17. Laurent, C. E., Delfino, F. J., Cheng, H. Y. & Smithgall, T. E. The human c-Fes tyrosine kinase binds tubulin and microtubules through separate domains and promotes microtubule assembly. *Mol. Cell. Biol.* **24**, 9351–9358 (2004).
18. Condorelli, F. *et al.* Role of the Non-Receptor Tyrosine Kinase Fes in Cancer. *Curr. Med. Chem.* **18**, 2913–2920 (2011).
19. Nomura, D. K., Dix, M. M. & Cravatt, B. F. Activity-based protein profiling for biochemical pathway discovery in cancer. *Nat. Rev. Cancer* **10**, 630–638 (2010).
20. Knight, Z. A. & Shokat, K. M. Chemical Genetics: Where Genetics and Pharmacology Meet. *Cell* **128**, 425–430 (2007).
21. Weiss, W. A., Taylor, S. S. & Shokat, K. M. Recognizing and exploiting differences between RNAi and small-molecule inhibitors. *Nat. Chem. Biol.* **3**, 739–744 (2007).
22. Karaman, M. W. *et al.* A quantitative analysis of kinase inhibitor selectivity. *Nat. Biotechnol.* **26**, 127–132 (2008).
23. Hellwig, S. *et al.* Small-molecule inhibitors of the c-Fes protein-tyrosine kinase. *Chem. Biol.* **19**, 529–540 (2012).
24. Bunnage, M. E., Chekler, E. L. P. & Jones, L. H. Target validation using chemical probes. *Nat. Chem. Biol.* **9**, 195–199 (2013).
25. Simon, G. M., Niphakis, M. J. & Cravatt, B. F. Determining target engagement in living systems. *Nat. Chem. Biol.* **9**, 200–205 (2013).
26. Zhao, Q. *et al.* Broad-spectrum kinase profiling in live cells with lysine-targeted sulfonyl fluoride probes. *J. Am. Chem. Soc.* **139**, 680–685 (2017).
27. Liu, Q. *et al.* Developing irreversible inhibitors of the protein kinase cysteinome. *Chem. Biol.* **20**, 146–159 (2013).
28. Lanning, B. R. *et al.* A road map to evaluate the proteome-wide selectivity of covalent kinase inhibitors. *Nat. Chem. Biol.* **10**, 760–767 (2014).
29. Zhao, Z., Liu, Q., Bliven, S., Xie, L. & Bourne, P. E. Determining Cysteines Available for Covalent Inhibition

Across the Human Kinome. *J. Med. Chem.* **60**, 2879–2889 (2017).
30. Garske, A. L., Peters, U., Cortesi, A. T., Perez, J. L. & Shokat, K. M. Chemical genetic strategy for targeting protein kinases based on covalent complementarity. *Proc. Natl. Acad. Sci. U. S. A.* **108**, 15046–15052 (2011).
31. Koch, A., Rode, H. B., Richters, A., Rauh, D. & Hauf, S. A chemical genetic approach for covalent inhibition of analogue-sensitive Aurora kinase. *ACS Chem. Biol.* **7**, 723–731 (2012).
32. Kung, A. *et al.* A Chemical-Genetic Approach to Generate Selective Covalent Inhibitors of Protein Kinases. *ACS Chem. Biol.* **12**, 1499–1503 (2017).
33. Backus, K. M. *et al.* Proteome-wide covalent ligand discovery in native biological systems. *Nature* **534**, 570–574 (2016).
34. Barf, T. & Kaptein, A. Irreversible protein kinase inhibitors: Balancing the benefits and risks. *J. Med. Chem.* **55**, 6243–6262 (2012).
35. Seeliger, M. A. *et al.* High yield bacterial expression of active c-Abl and c-Src tyrosine kinases. *Protein Sci.* **14**, 3135–3139 (2005).
36. Dann, S. G. *et al.* P120 catenin is a key effector of a Ras-PKCε oncogenic signaling axis. *Oncogene* **33**, 1385–1394 (2014).
37. Lebraud, H. *et al.* In-gel activity-based protein profiling of a clickable covalent ERK1/2 inhibitor. *Mol. BioSyst.* **12**, 2867–2874 (2016).
38. Cohen, M. S., Hadjivassiliou, H. & Taunton, J. A clickable inhibitor reveals context-dependent autoactivation of p90 RSK. *Nat. Chem. Biol.* **3**, 156–160 (2007).
39. Tan, L. *et al.* Structure-guided development of covalent TAK1 inhibitors. *Bioorganic Med. Chem.* **25**, 838–846 (2017).
40. Fabbro, D., Cowan-Jacob, S. W. & Moebitz, H. Ten things you should know about protein kinases: IUPHAR Review 14. *British Journal of Pharmacology* **172**, 2675–2700 (2015).
41. Craig, A. W. B., Zirngibl, R. & Greer, P. Disruption of coiled-coil domains in Fer protein-tyrosine kinase abolishes trimerization but not kinase activation. *J. Biol. Chem.* **274**, 19934–19942 (1999).
42. Islam, K. Allele-specific chemical genetics: Concept, strategies, and applications. *ACS Chem. Biol.* **10**, 343–363 (2015).
43. Bishop, A. C. *et al.* A chemical switch for inhibitor-sensitive alleles of any protein kinase. *Nature* **407**, 395–401 (2000).
44. Moyer, T. C., Clutario, K. M., Lambrus, B. G., Daggubati, V. & Holland, A. J. Binding of STIL to Plk4 activates kinase activity to promote centriole assembly. *J. Cell Biol.* **209**, 863–878 (2015).
45. Zhang, C. *et al.* A second-site suppressor strategy for chemical genetic analysis of diverse protein kinases. *Nat. Methods* **2**, 435–441 (2005).
46. Au-Yeung, B. B. *et al.* A genetically selective inhibitor demonstrates a function for the kinase Zap70 in regulatory T cells independent of its catalytic activity. *Nat. Immunol.* **11**, 1085–1092 (2010).
47. Weerapana, E., Simon, G. M. & Cravatt, B. F. Disparate proteome reactivity profiles of carbon electrophiles. *Nat. Chem. Biol.* **4**, 405–407 (2008).
48. Ogasawara, D. *et al.* Rapid and profound rewiring of brain lipid signaling networks by acute diacylglycerol lipase inhibition. *Proc. Natl. Acad. Sci.* **113**, 26–33 (2016).
49. Rosenberger, A. F. N. *et al.* Protein kinase activity decreases with higher braak stages of Alzheimer's disease pathology. *J. Alzheimer's Dis.* **49**, 927–943 (2015).
50. Borrelli, K. W., Benjamin, C. & Victor, G. Exploring hierarchical refinement techniques for induced fit docking with protein and ligand flexibility. *J. Comput. Chem.* **31**, 1224–1235 (2010).
51. Baggelaar, M. P. *et al.* Highly Selective, Reversible Inhibitor Identified by Comparative Chemoproteomics Modulates Diacylglycerol Lipase Activity in Neurons. *J. Am. Chem. Soc.* **137**, 8851–8857 (2015).
52. Florea, B. I. *et al.* Activity-based profiling reveals reactivity of the murine thymoproteasome-specific subunit β5t. *Chem. Biol.* **17**, 795–801 (2010).
53. Wong, J. C. *et al.* Pharmacokinetic optimization of class-selective histone deacetylase inhibitors and identification of associated candidate predictive biomarkers of hepatocellular carcinoma tumor response. *J. Med. Chem.* **55**, 8903–8925 (2012).
54. Ménard, D. *et al.* Novel potent BRAF inhibitors: Toward 1 nM compounds through optimization of the central phenyl ring. *J. Med. Chem.* **52**, 3881–3891 (2009).